European Journal of Pharmaceutical Sciences 213 (2025) 107238

Contents lists available at ScienceDirect

European Journal of Pharmaceutical Sciences

journal homepage: www.elsevier.com/locate/ejps

Photodegradation of the antibacterial, antifungal and antiprotozoal drug candidate 2-(2-nitrovinyl) furan (G-0) in solid inclusion complexes with β-cyclodextrin derivatives: Characterization by NMR spectroscopy and in silico toxicity screening

Vivian Ruz Sanjuan [a,1], Antonio Gilberto Ferreira [b], Enoel Hernández Barreto [c], Guy Van den Mooter [d], Mirtha Mayra González Bedia [e], Eryvaldo Socrates Tabosa do Egito [f,*], Anselmo Gomes de Oliveira [a,*]

[a] São Paulo State University (UNESP), Graduate Program in Pharmaceutical Sciences, School of Pharmaceutical Sciences, Rodovia Araraquara-Jaú, km 01, 14, Araraquara, SP 800-903, Brazil
[b] Laboratory of Nuclear Magnetic Resonance, Department of Chemistry, Federal University of São Carlos (UFSCar), Box 676, Washington Luiz s/n, km 235, São Carlos, SP 13.565-905, Brazil
[c] Instituto Superior Politécnico de Malanje. Rúa Sacadura Cabral, S/N, Centro Urbano de Malanje, Malanje, Angola
[d] Drug Delivery and Disposition, Department of Pharmaceutical and Pharmacological Sciences. O&N2 Herestraat 49-Box 921, University of Leuven (KULeuven), Leuven BE-3000, Belgium
[e] Pharmacy Department, Chemistry and Pharmacy Faculty, Central University of Las Villas, Carretera a Camajuaní km 5 ½, Villa Clara 54830, Cuba
[f] Pharmacy Department, Graduate Program in Health Sciences, Federal University of Rio Grande do Norte (UFRN), Rua Gal. Gustavo Cordeiro de Farias, s/n, Petrópolis, Natal, RN 59010-180, Brazil

ARTICLE INFO

Keywords:
2-(2-nitrovinyl)furan
Inclusion complexes
Photodegradation
NMR spectroscopy
In silico toxicity
Toxtree

ABSTRACT

This work aimed to evaluate the effect of inclusion complex (IC) formation between the drug candidate 2-(2-nitrovinyl) furan (G-0) and hydroxypropyl β-cyclodextrin (HP-β-CD) or sulfobutylether β-cyclodextrin (SBE-β-CD) on the drug's photostability under light exposure. Freeze-dried cyclodextrin inclusion complexes (ICs) and their corresponding physical mixtures were subjected to standardized forced irradiation and light exposure conditions according to ICH guidelines. Kinetic analysis suggested potential alterations in photodegradation pathways. The HPLC chromatographic profile of the ICs exhibited a distinct impurity pattern compared to the physical mixtures, while the profiles of the two ICs were similar. The main photodegradation product (PD1) was identified with a retention time of 5.4 min and a maximum absorption wavelength (λ_{max}) of 330 nm. PD1 was isolated using High-Performance Liquid Chromatography with diode array detection (HPLC-DAD) and further characterized through Nuclear Magnetic Resonance (NMR) spectroscopy. Combining 1D (^{1}H NMR, ^{13}C {^{1}H}) and 2D (COSY, HSQC and HMBC) NMR measurements revealed the presence of two substances in equilibrium, identified as (2Z,4Z)-5-nitropenta-2,4-dienoic acid (NPDA) and its corresponding salt. The hazard classification of NPDA was assessed following ICH M7 guidelines using QSAR and expert rule-based toxicity screening methods, providing insights into its potential risk profile.

Abbreviations: G-0, 2-(2-Nitrovinyl)furan; IC, Inclusion complex; FDIC G-0/HP-β-CD, Freeze-dried inclusion complex of G-0 in hydroxypropyl-β-cyclodextrin; FDIC G-0/SBE-β-CD, Freeze-dried inclusion complex of G-0 in sulfobutylether-β-cyclodextrin; NPDA, (2Z,4Z)-5-nitropenta-2,4-dienoic acid.

* Corresponding authors.
E-mail addresses: vivianr@uclv.edu.cu (V.R. Sanjuan), giba_04@yahoo.com.br (A.G. Ferreira), ehb7708@gmail.com (E.H. Barreto), guy.vandenmooter@kuleuven.be (G.V. den Mooter), mmayra@uclv.edu.cu (M.M.G. Bedia), socrates@ufrnet.br (E.S.T. do Egito), anselmo.gomes@unesp.br (A.G. de Oliveira).
[a] (V.R.S.) Present address: Pharmacy Department, Chemistry and Pharmacy Faculty, Central University of Las Villas, Carretera a Camajuaní km 5 ½, Villa Clara 54830, Cuba

https://doi.org/10.1016/j.ejps.2025.107238
Received 10 March 2025; Received in revised form 17 August 2025; Accepted 18 August 2025
Available online 18 August 2025

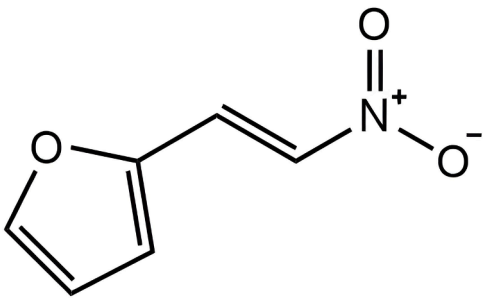

Fig. 1. Chemical structure of 2-(2-nitrovinyl)furan (G-0).

1. Introduction

Cyclodextrins have been extensively studied for their ability to enhance the physical and chemical stability of drugs through the formation of inclusion complexes (Ruz et al., 2015; Popielec and Loftsson, 2017; Yuan et al., 2018). 2-(2-Nitrovinyl) furan (G-0) (Fig. 1), a derivative of 2-furylethylene, has demonstrated a broad spectrum of biological activities, including anticoccidial (Olazábal-Manso et al., 2002), antileishmanial and antichagasic effects (Sifontes-Rodríguez et al., 2015; Sifontes-Rodríguez, 2017).

Additionally, G-O exhibits potent antibacterial activity against various pathogens, including *Escherichia coli* (Ajiboye, 2018; Alabi and Owolabi, 2012), *Salmonella typhimurium, Staphylococcus aureus, Pseudomonas aeruginosa* (Alabi and Owolabi, 2012), *Klebsiella pneumoniae, Staphylococcus epidermidis, Bacillus cereus, Bacillus subtilis* and *Pseudomonas syringae* (Alabi and Hassan, 2014). Its antifungal activity has also been reported against *Candida albicans* (Alabi and Hassan, 2014; Ruz--Sanjuan et al., 2020) and *Candida krusei* (Ruz-Sanjuan et al., 2020),

Additional toxicity studies were conducted on the drug candidate 2-(2-nitrovinyl)furan, including an *in vitro* micronucleus assay (Gonzalez Borroto et al., 2003), sister chromatid exchange, SOS induction assay in *E. coli*, and the Ames test, all of which indicated no mutagenic or genotoxic effects (González Borroto et al., 2001; González Borroto et al., 2005). Despite its broad-spectrum antimicrobial activity, the chemical instability and sublimation capacity of 2-(2-nitrovinyl)furan have posed significant challengers to the development of a successful formulation.

Previously, we demonstrated that this compound could be encapsulated within the hydrophobic cavities of 2-HP-β-CD and SBE-β-CD using the freeze-drying method (Ruz et al., 2012). Recent studies have focused on enhancing its physical stability to mitigate sublimation (Ruz et al., 2015), as well as conducting accelerated chemical stability tests. These investigations revealed that the inclusion complexes formed with both cyclodextrins exhibited superior performance compared to their corresponding physical mixtures (Ruz-Sanjuan et al., 2020).

The intrinsic photostability of the molecular complexes, on the other hand, must be evaluated to demonstrate whether these complexes can protect G-0 from light without unacceptable changes or if light-resistant packaging is necessary. Light exposure is well known to cause chemical alterations in Active Pharmaceutical Ingredients (APIs) and their final products. Photodegradation can manifest as changes in sample color, bleaching, alterations in dissolution rate, or loss of activity. In some cases, photoreactions may generate intermediates or degradation products with increased toxicity or induce Reactive Oxygen Species (ROS), leading to chain reactions that may harm human tissues.

The extent of photodegradation varies significantly among substances. While some compounds exhibit slight degradation over weeks of light exposure, others have photochemical half-lives lasting only a few minutes. Light-sensitive drugs can be degraded by sunlight (ultraviolet light) or artificial light (*e.g.*, fluorescent light), with the latter being less energetic (Bhalekar et al., 2008). Photochemical decomposition typically occurs due to light absorption in the 300–500 nm range. In this context, the ICH guidelines recommend conducting forced and confirmatory studies using both natural and artificial light source (ICH 1996).

For stability testing, key experimental factors include ensuring proper mixing of liquids, uniform stirring of solids, and maintaining a consistent sample temperature. High-intensity photon sources are required for stress testing during the preformulation stage to evaluate the material sensitivity and identify potential degradation products for analytical purposes (Moore, 2004). The photochemical degradation process is highly dependent on the spectral properties of the drug or chemical system and the spectral distribution of the light source.

Certain chemical structures are particularly prone to photoreactions, including $C = C$ double bonds (which may undergo E/Z isomerization, polar addition, or cycloaddition), five-membered heterocyclic rings (which are susceptible to rearrangement), vinyl furans (which can dimerize) (D'Auria et al., 2000), and N-oxides (which may undergo electrolytic reactions) (Bhalekar et al., 2008). Photodegradation can occur directly or indirectly; in the latter case, energy absorbed by an excipient, impurity, or degradation product (known as photosensitizer) may transfer energy without itself being altered or, in some cases, degrade. Excipients can thus initiate, propagate, or participate in photochemical reactions.

If degradation products are observed, their careful analysis, identification and characterization are essential (ICH Q3A, ICH, Q3A (R2) 2006). Therefore, the main objective of this study was to investigate the photodegradation of G-0 in the molecular inclusion complexes with cyclodextrin derivatives in the solid state, following ICH Q1B guidelines. The study also aimed to detect, isolate, and characterize the primary degradation product using HPLC-DAD and NMR spectroscopy.

The need to estimate the toxicological risk of chemicals in domains such as pharmaceutical, nutrition, and cosmetics has driven the adoption of computational tools to reduce the time and cost of analyses and experimental research involving animals, while also addressing ethical considerations. The annual economic burden of producing and maintaining animal models for *in vivo* toxicological assessment is substantial (Bottini and Hartung, 2009).

According to the ICH M7 guideline, structure-based computational methods or QSAR analyses can be employed to estimate the toxic potential when adequate experimental data are unavailable. These methods enable classification into Class 3, 4, or 5, under the "Impurities Classification" related to Mutagenic and Carcinogenic Potential and Resulting Control Actions (ICH M7 2017). *In silico* toxicology uses computational resources, such as data, methods, software, to estimate the toxic potential of a chemical. It complements *in vitro* and *in vivo* tests by offering quantitative or qualitative predictions of adverse effects, referred to as endpoints (Raies and Bajic, 2016).

A variety of computational methods are currently available to predict chemical toxicity (Raies and Bajic, 2016; Schmidt, 2021), and their implementation must adhere to established procedures and principles (Amberg et al., 2016). These methods generally fall into two categories: expert rules-based approaches and statistical (QSAR model) approaches (ICH M7 2017). Recent advances have combined these methods or introduced new models (Fjodorova and Novic, 2012; Kolarević et al., 2016; Luechtefeld et al., 2018; Manganelli et al., 2016; Tourneix et al., 2010; Wang et al., 2019; Yeni and Merdekawati, 2018; Zhuang et al., 2018) while the benefits of using read-across techniques and *in silico* tools have also been evaluated (Stanton and Kruszewski, 2016). However, limitations of some widely used QSAR methods, particularly estimating the irritating or corrosive potential of chemical products on the skin, have been reported (Verheyen et al., 2017).

Based on this concept, the secondary objective of our study was to perform computational toxicology predictions for the isolated photoproduct, adhering to the ICH M7 guideline for hazard classification (ICH M7 2017). This analysis employed statistical methods (or QSAR models), expert rules (structural alerts), and read-across assessments. The combination of these approaches enhances the reliability of the predictions (Myatt et al., 2018). Additional toxicity predictions,

including assessments for skin sensitization, were also conducted.

2. Materials and methods

2.1. Drug and reagents

The bulk drug and reference standard of 2-(2-nitrovinyl) furan (G-0) (>99.5 %, MW= 139.1 g/mol) were kindly provided by the Centro de Bioactivos Químicos (Villa Clara, Cuba) and synthesized according to the reported method (Olazábal-Manso et al., 2002). Hydroxypropyl-β-cyclodextrin (Trappsol®, Pharmaceutical grade) was purchased from CTD, Inc., USA, and sulfobutylether-β-cyclodextrin (Captisol®, Research grade) obtained from CyDex Pharmaceuticals Inc., USA.

Acetonitrile (HPLC grade) and deuterated solvent CD_3CN (99.8 % D), were sourced from Sigma-Aldrich, Germany. Deionized water was prepared using a MilliQ water purification system (Merck, Germany). All other reagents used in this study were of analytical grade.

2.2. Photodegradation methodology

2.2.1. Preparation of the inclusion complexes by freeze-drying

Freeze-dried inclusion complexes were obtained according to a previously reported method (Ruz et al., 2012), with slight modifications. Briefly, a saturated solution was prepared by dissolving each cyclodextrin (CD) derivative in 50 mL of deionized water, followed by the addition of G-0 in an equimolar amount. The resulting suspension was stirred horizontally at 21 ± 1 °C for 48 h to allow equilibrium formation of the drug-CD inclusion complex.

The dispersion was filtered through 0.22-micron membranes, dispensed into 1 mL glass vials, frozen at −40 °C and lyophilized using a JJ Cientifica® lyophilizer (São Paulo, Brazil) for 24 h at −30 °C and 150 mmHg.

2.2.2. Irradiation conditions

2.2.2.1. Forced irradiation using a UVC chamber. For the irradiation of solid inclusion complexes (ICs) or corresponding physical mixtures (PMs), the contents of each vial were spread homogeneously on glass Petri dishes ($N = 3$) to form a layer of less than 1 mm in thickness. The samples were placed in a closed chamber internally coated with mirrors and positioned 10 cm away from the lamp. The light source was a UV lamp (SM 808, Zhejiang, China), emitting radiation at 254 nm, positioned horizontally within the chamber. The temperature during irradiation was controlled at 20 ± 1 °C, and activated silica gel was placed inside the chamber to prevent moisture absorption by the samples.

To ensure uniform light exposure, the samples were shaken daily. Sampling was conducted at 12-hour intervals until 50 % degradation was achieved. The physical mixtures were analyzed as a control for comparison.

2.2.2.2. Irradiation using an ICH photostability chamber. The behavior of ICs under conditions established by the International Council for Harmonisation of Technical Requirements for Pharmaceuticals for Human Use (ICH) Q1B guideline (ICH 1996) was investigated using a photostability climatic chamber (Mecalor EC/0.2/R-F, Mecalor Thermal Engineering Solutions Ltd., Brazil). The solid complexes were exposed to a combination of cool white fluorescent light (visible spectrum) and a UV lamp (UVA), corresponding to Photostability Testing-Option 2.

The light source emitted a spectral distribution between 320 and 400 nm, with a peak emission energy at 350–370 nm. The samples were illuminated to achieve 1.2 million lux-hours visible light exposure and a near-ultraviolet energy of 200 W-hours/m^2. The chamber was equipped with an integrated radiometer and lux meter to measure the UV radiation and illuminance, respectively. The temperature was maintained at 25 °C throughout the exposure.

2.2.3. Preparation of irradiated samples for HPLC analysis

The drug inclusion complexes (ICs) or physical mixtures (PMs) with cyclodextrins (CDs), as well as their degradation products, were analyzed at their maximum absorption wavelengths. Approximately 10 mg of solid IC or PM was accurately weighed and dissolved volumetrically in 25 mL of the mobile phase. The solutions were filtered using PTFE 0.45 μm filters (Chromafil®).

A 20 μL aliquot of the filtered solution was injected into the chromatograph for analysis. A calibration curve for G-0 (used as the reference standard) was prepared within a concentration range of 1 to13 μg/mL to facilitate quantification.

2.2.3.1. Chromatographic conditions. An Agilent Technologies 1220 HPLC apparatus, equipped with a Diode Array Detector (DAD 1220 Infinity), an automatic injector, and a quaternary pump was employed for the analysis. Separation was achieved using an Agilent Zorbax ODS column (250×4.6 mm, 5 μm) with an Agilent Zorbax guard column ODS (12.5 × 4.6, 5 μm). The mobile phase consisted of acetonitrile and water 80:20 (v/v), delivered isocratically at a flow rate of 0.5 mL/min at room temperature. The injection volume was set at 20 μL, with detection performed at a wavelength of 351 nm. The run time for each analysis was 15 min. A multispectral diode array detector was utilized for the detection of photodegradation products, scanning from 200 to 400 nm at a rate of one spectrum per second with a resolution of 1.2 nm.

2.2.4. Kinetic analysis of photodegradation

The kinetic curves were obtained by plotting the remaining G-0 concentration against time. Photodegradation was monitored for at least three half-lives for all samples. The degradation rate constants and respective half-lives were determined by iterative analysis using SigmaPlot for Windows 10.0 (Systat Software, Inc.). Statistical comparisons of the photodegradation kinetic curves of G-0 in inclusion complexes *versus* their corresponding physical mixtures were performed using a *t*-test with a 95 % confidence interval, analyzed with Statistical software v.10.0 (StatSoft Inc., U.S.A).

2.2.5. Isolation and characterization of photodegradation products

2.2.5.1. Sample clean-up. To remove potential cyclodextrins interferences prior to spectroscopic analysis, a Phenomenex® C18 cartridge (55 μm, 70 Å) was utilized. The cartridge was preconditioned by washing with 5 mL of acetonitrile (HPLC grade) and subsequently activated with 5 mL of deionized water. The contents of two vials containing the solid irradiated complex were fully dissolved in 2 mL of deionized water and loaded onto the cartridge. Cyclodextrins were eluted with 5 mL of deionized water, while organic compounds were retained. The retained compounds were then eluted with 2 mL of an acetonitrile-water mixture (80:20, v/v) and collected in amber vials. The eluted fraction was stored at −40 °C for subsequent separation and analysis. Pressure was applied during the clean-up procedure to expedite the process.

2.2.5.2. Isolation of photoproducts in an analytical column. The organic fraction was filtered through a PTFE 0.45 μm filter, (Chromafil®) and analyzed using a Shimadzu LC-10AD High-Performance Liquid Chromatography system (Shimadzu, Japan). Separation was performed on a C18 column (250 mm x 4.6 mm, 5 μm; Agilent Technologies) with a mobile phase consisting of acetonitrile and water (80:20, v/v), in isocratic mode at a flow rate of 0.5 mL/min. The injection volume was 50 μL, with a runtime of 15 min at 25 °C.

Photoproducts were collected based on retention times and maximum absorption wavelengths, with a collection limit set at 1000 milliabsorbance units (mAU). Collected fractions were dried under a

Table 1
G-0 content in dark controls of inclusion complexes and physical mixtures for both cyclodextrins.

Sample	G-0 content (%, w/w)	
	Time 0	48 h
FDIC G-0/HP-β-CD IC	2.104 ± 0.115	1.972 ± 0.062
PM G-0/HP-β-CD	1.842 ± 0.086	1.447 ± 0.206 *
FDIC G-0/SBE-β-CD IC	2.203 ± 0175	2.104 ± 0.167
PM G-0/SBE-β-CD	2.535 ± 0.078	2.335 ± 0.398

Data are expressed as mean ± standard deviation ($n = 3$).
* Significant statistical difference, $p < 0.05$. FDIC: Freeze-dried inclusion complex; PM: Physical mixture.

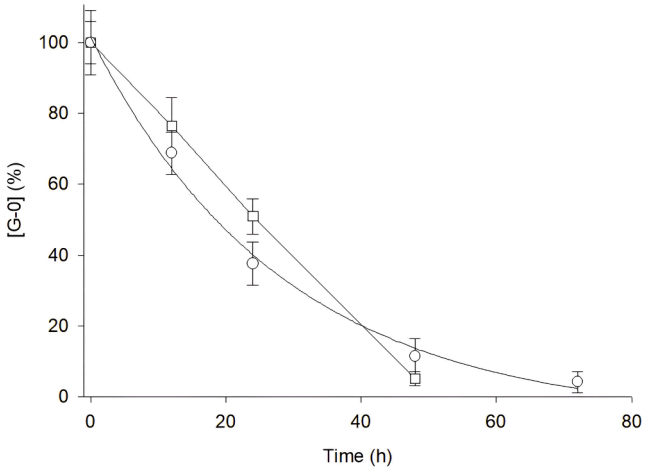

Fig. 2. Photodegradation kinetics of G-0 in freeze-dried inclusion complexes (FDIC) and physical mixtures (PM) with HP-β-CD. Key: (□) PM HP-β-CD), (○) FDIC HP-β-CD. The black lines represent the fit of the experimental data using zero-order and first-order kinetic models for PM and FDIC, respectively. Photodegradation kinetics were monitored for at least three half-lives.

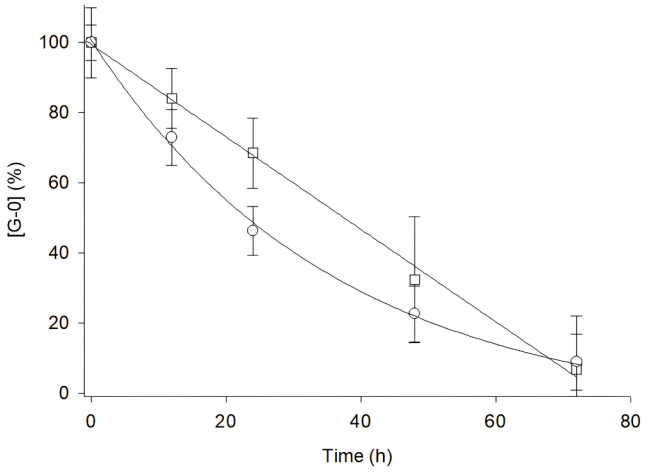

Fig. 3. Photodegradation kinetics of G-0 in Freeze-dried Inclusion Complex (FDIC) and physical mixtures (PM) with SBE-β-CD components. Key: (□) PM SBE-β-CD, (○) FDIC SBE-β-CD. The black lines represent the fit of the experimental data to zero-order and first-order kinetic models for PM and FDIC, respectively. Photodegradation kinetics were monitored for at least three half-lives.

nitrogen atmosphere using a SOLAB Nitrogen Evaporator Sample Concentrator (SOLAB, Brazil) and subsequently reconstituted with appropriate volumes of deuterated acetonitrile. Samples corresponding

Table 2
Kinetic parameters determined from photodegradation of G-0 in freeze-dried inclusion complexes (FDIC) and physical mixtures (PM) with HP-β-CD and SBE-β-CD. Data were calculated by iteration using Statistica 10.0 software.

Kinetic parameters	G-0/HP-β-CD		G-0/SBE-β-CD	
	PM	FDIC	PM	FDIC
Reaction order	Zero	First	Zero	First
R^2	0.999	0.997	0.995	0.999
k (h^{-1})	–	0.0352	–	0.0278
k (% h^{-1})	1.982	–	1.319	–
$t_{1/2}$ (h)	25.23	23.90	37.90	24.93

Key: (FDIC) Freeze-dryed Inclusion Complex; (PM) Physical Mixtures.

to the primary photoproduct (PD1) were pooled to ensure sufficient quantity for analysis. The final solution, containing 600 μL of deuterated solvent, was transferred to a 5-mm NMR glass tube and protected from light until analysis.

2.2.5.3. Characterization of the main photoproduct (PD1) by nuclear magnetic resonance spectroscopy. The characterization of PD1 was conducted using a Bruker Avance III spectrometer (Karlsruhe, Germany), operating at a magnetic field strength of 14.1 T (600 MHz for proton frequency). The instrument was equipped with a 5 mm TXI cryoprobe head for ^{1}H, ^{13}C, and ^{15}N, and experiments were performed at 298 K using deuterated acetonitrile (CD3CN) as both solvent and internal reference.

^{1}H NMR spectra were acquired using the noesypr1d pre-saturation pulse sequence (Bruker terminology). The acquisition parameters were as follows:

- Number of scans (n_s): 8
- Acquisition time: 3.02 s
- Relaxation delay (d_1): 3.0 s
- Pre-saturation time (d_8) = 0.5 s
- Spectral width (SW) = 18.03 ppm
- Number of data points (TD) = 65 K
- Receiver gain (RG) = 64.

The $^{13}C\{^{1}H\}$ spectra were obtained using the zgpg30 power-gated decoupling pulse sequence (Bruker terminology) with these parameters:

- Number of scans (n_s): 70
- Acquisition time: 0.47 s
- Relaxation delay (d_1): 0.1 s
- Spectral width (SW) = 57.8 ppm
- Receiver gain (RG) = 203
- Number of data points (TD) = 32 K
- Line broadening (LB): 3 Hz

Homonuclear Correlation Spectroscopy (COSY) spectra were recorded using the cosygpprqf pulse sequence with HDO pre-saturation (Bruker terminology). Parameters included:

- Number of scans (n_s): 6
- Spectral width (SW): 18.03 ppm in both dimensions
- Relaxation delay (d_1): 1,0 s
- Data points (TD): 175 K in F_1 (TDF1) and 4 K in F_2 (TDF2) = 4 K

Heteronuclear Single Quantum Coherence Spectroscopy (HSQC) were acquired using the hsqcetgpprsisp2.2 pulse sequence in echo-anti-echo phase-sensitive mode with HDO pre-saturation (Bruker terminology). Acquisition parameters were:

- Number of scans (n_s): 8
- Spectral width (SW): 18.03 ppm (proton) and 238.31 ppm (carbon)

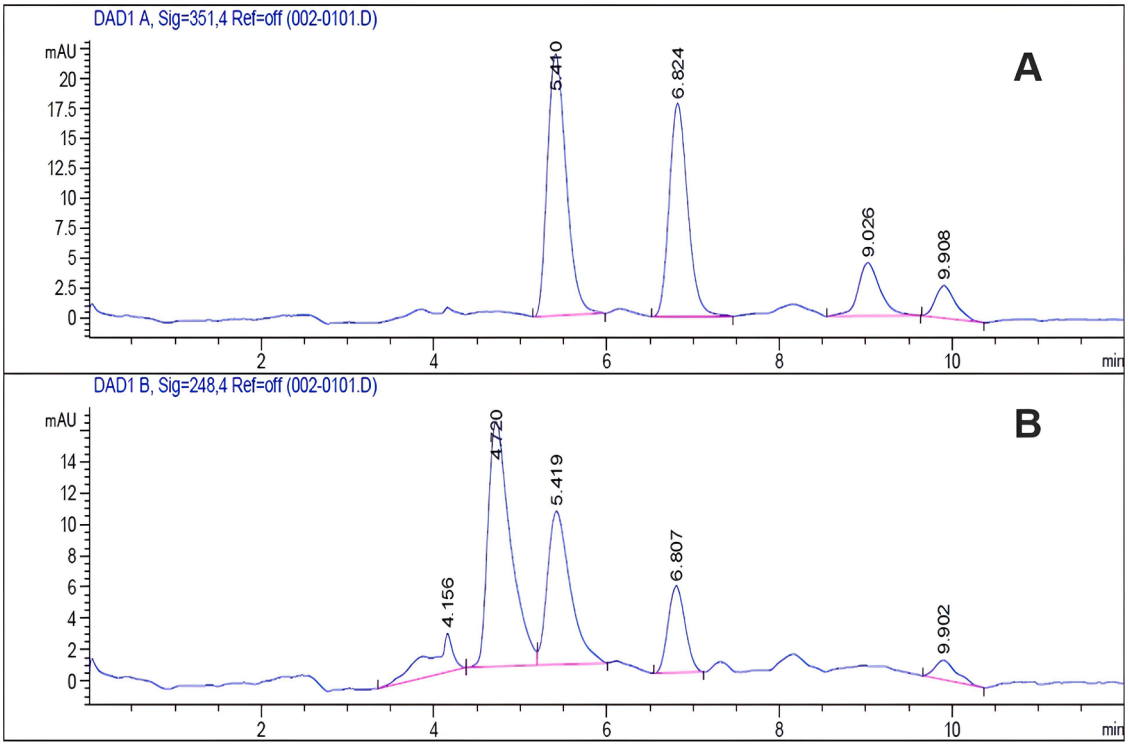

Fig. 4. Representative chromatograms of FDIC G-0/SBE-β-CD samples after 48 h of forced irradiation conditions (UVC). Detection wavelengths: (**A**) 351 nm and (**B**) 248 nm.

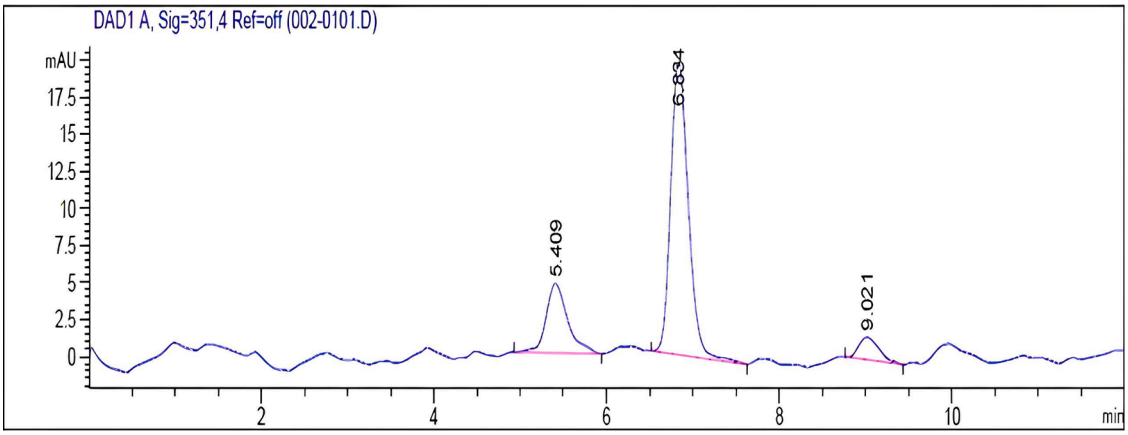

Fig. 5. Chromatogram of an FDIC G-0/SBE-β-CD sample after irradiation under kinetic experimental condition in a photostability chamber (ICH–Option 2). Detection wavelength: 351 nm.

- Relaxation delay (d_1): 1.0 s
- Data points (*TD*): 256 K in F_1 (TDF1) and 4 K in F_2 (TDF2)
- Apodization function: QSINE with sideband suppression (SSB=3)

2.3. *In silico toxicity screening for the obtained photoproduct*

The toxicological profile of (2Z,4Z)-5-nitropenta-2,4-dienoic acid (NPDA) was assessed using various computational methods. The SMILES code was generated using the JSME molecular editor (Bienfait and Ertl, 2013), available at (https://jsme-editor.github.io/. This code was then input into either local PC-based software or web-based predictive tools, depending on the specific method employed. Details of the software used are described below.

2.3.1. *Toxtree 3.1.0*

The free software Toxtree was used to estimate the toxic hazard based on multiple predictive models, including Cramer rules (with extensions), Verhaar scheme, carcinogenicity (genotoxic and non-genotoxic), *in vitro* mutagenicity (AMES test), skin sensitization reactivity domains, structure alerts for *in vivo* micronucleus assay in rodents, protein binding alerts, and DNA binding alerts. (Downloaded from: http://toxtree.sourceforge.net/)

2.3.2. *OSIRIS property explorer*

This application provides default risk assessments for mutagenicity, tumorigenicity, irritating effects, and reproductive toxicity. (Downloaded from: https://www.organic-chemistry.org/prog/peo/)

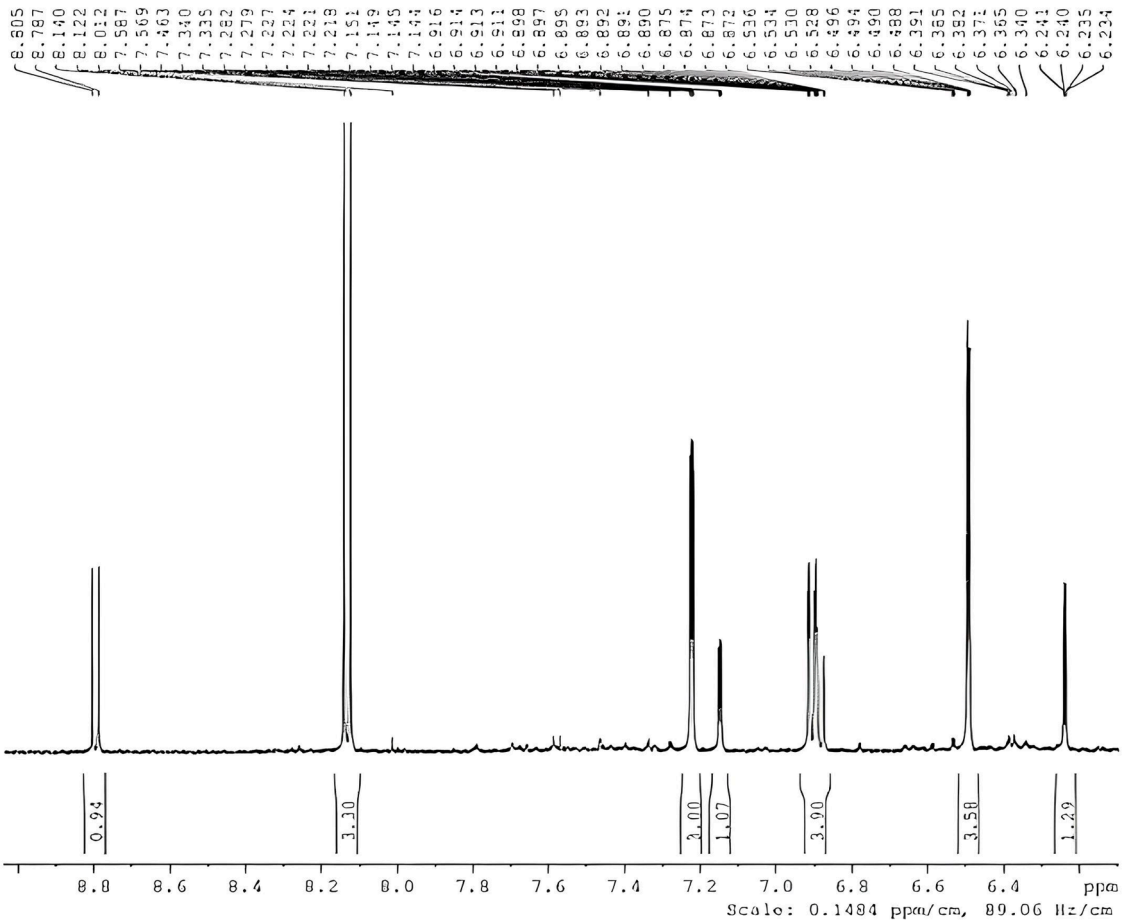

Fig. 6. Expanded ^{1}H NMR spectrum of PD1 dissolved in deuterated acetonitrile (CD_3CN).

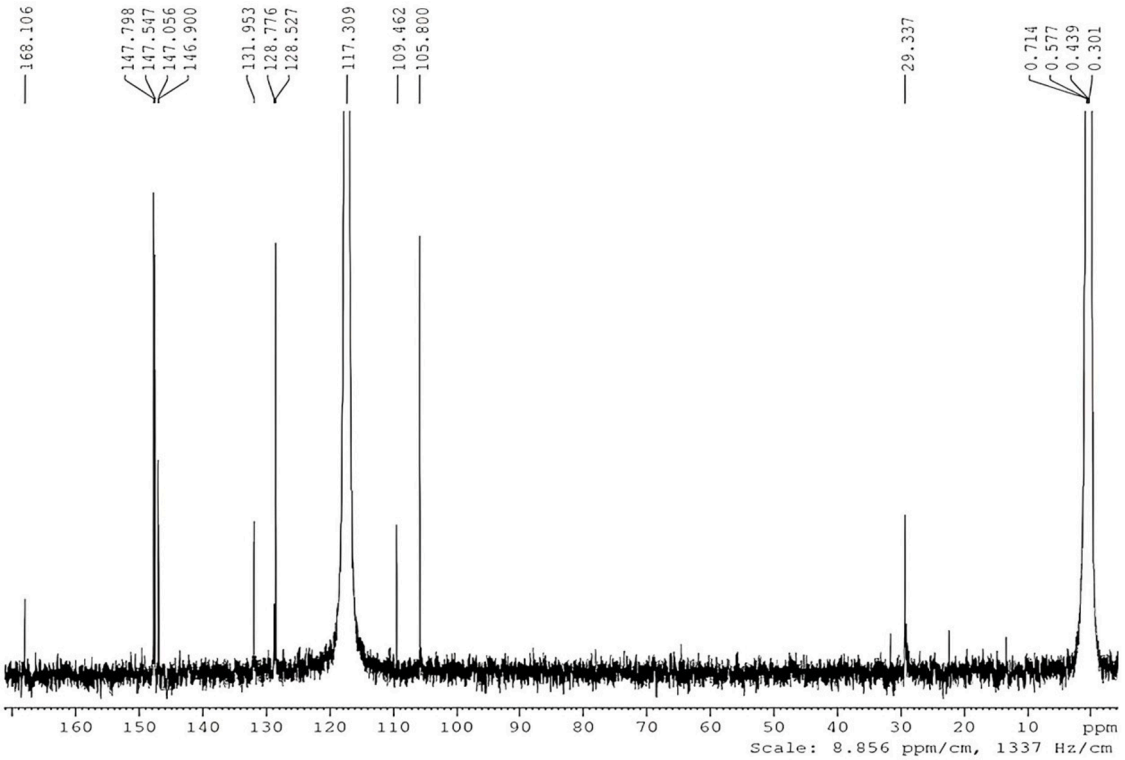

Fig. 7. $^{13}C\{^{1}H\}$ NMR spectrum of PD1 dissolved in CD_3CN, highlighting signals corresponding to the analyzed compounds, impurities, and solvent-related peaks.

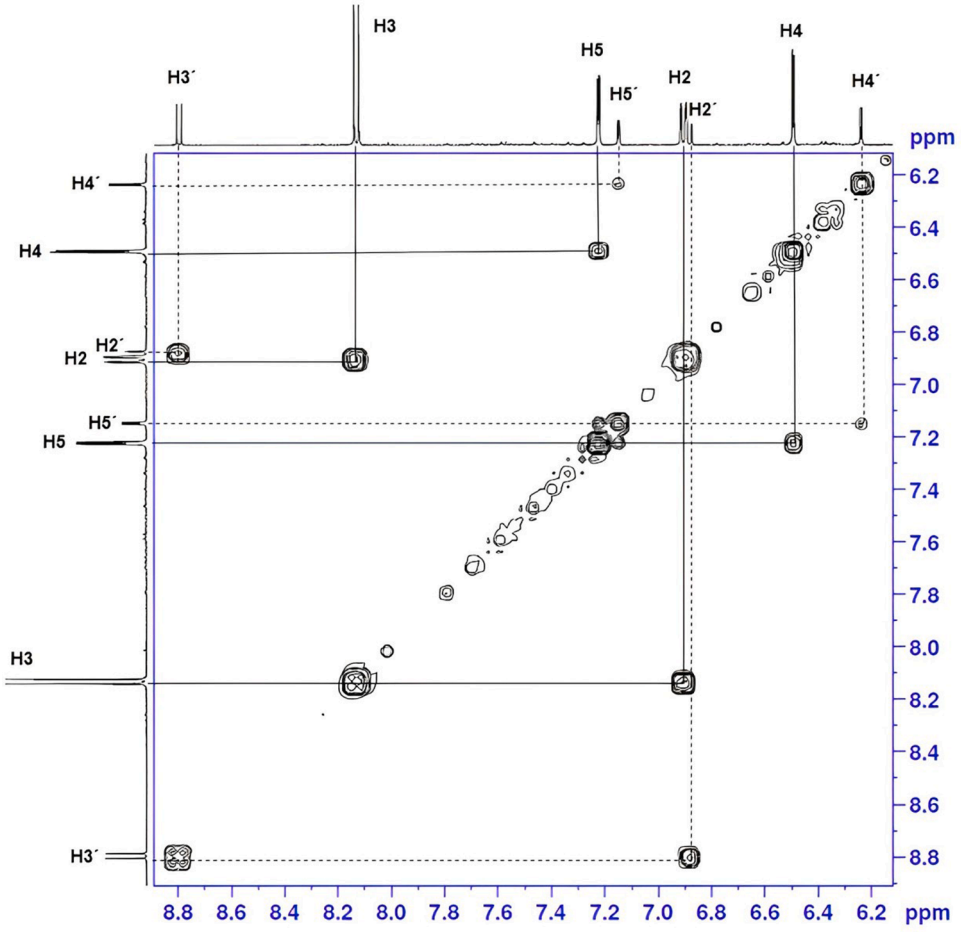

Fig. 8. $^{1}H–^{1}H$—COSY contour map for PD1 dissolved in CD_3CN. Continuous lines indicate correlations for the substance present in higher proportions, while dashed lines represent correlations for the substance in lower proportions.

2.3.3. pkCSM

pkCSM offers pharmacokinetic and toxicological predictions. For this study oral rat acute toxicity, oral rat chronic toxicity, skin sensitization, AMES toxicity, and hERG I inhibitor/hERG II inhibition were considered. (Online: http://bosig.unimelb.edu.au/pkcsm/prediction/)

2.3.4. preADMET

The preADMET online predictor was used to estimate AMES test results, carcinogenicity in mice and rats, and *in vitro* hERG inhibition. (Online: https://preadmet.bmdrc.kr/toxicity/).

2.3.5. T.E.S.T. 4.2.1

The software predicts mutagenicity and oral toxicity in rats (LD_{50}). (Downloaded from: https://www.epa.gov/chemical-research/toxicity-estimation-software-tool-test).

2.3.6. QSAR Toolbox 4.4.1

QSAR Toolbox was employed to predict toxic hazard classifications, alerts for carcinogenicity (genotoxic and non-genotoxic), DNA alerts for AMES, *CA*, and MNT (by OASIS), *in vitro* mutagenicity alerts (AMES and Micronucleus, by ISS), protein binding alerts for chromosomal aberration and skin sensitization (by OASIS), and protein binding alerts for GHS skin sensitization. (Downloaded from: https://qsartoolbox.org/download/).

2.3.7. ToxRead 0.23

It was utilized to predict mutagenicity, carcinogenicity, *in vitro* micronucleus assay results, and skin sensitization. (Downloaded from https://www.vegahub.eu/download/toxread-download/).

For comparative purposes, 2-(2-nitrovinyl)furan (G-0), a well-known non-mutagenic antimicrobial (CAS 699-18-3) from which the photodegradation product was derived via photolytic reaction, was subjected to the same predictive procedures.

3. Results and discussion

3.1. Effect of cyclodextrins on the G-0 photostability in solid state

The G-0 concentrations in the inclusion complexes (ICs) used as controls and maintained in dark environment did not show significant differences during the photodegradation assay (one way ANOVA, $p = 0.15$ for FDIC G-0/HP-β-CD; $p = 0.51$ for FDIC G-0/SBE-β-CD), indicating no degradation occurred in the controls under the experimental temperature conditions (Table 1).

The equivalent physical mixture used in dark controls (Table 1) showed a slightly difference in G-0 content between time 0 (t_0) and 48 h for PM G-0/HP-β-CD (one way ANOVA $p = 0.037$; $p < 0.05$). However, no degradation products were detected in the analysis of the physical mixtures. This observation may be attributed to minor sublimation of the drug or lack of homogeneity in the blends.

The results confirm the protective effect of cyclodextrins in stabilizing G-0 in the solid state under dark conditions. In contrast, the physical mixture (PM) of G-0/HP-β-CD showed a statistically significant reduction in drug content ($p < 0.05$), suggesting that the interaction between G-0 and HP-β-CD in the PM form may not provide adequate stabilization under these conditions. Conversely, no significant changes

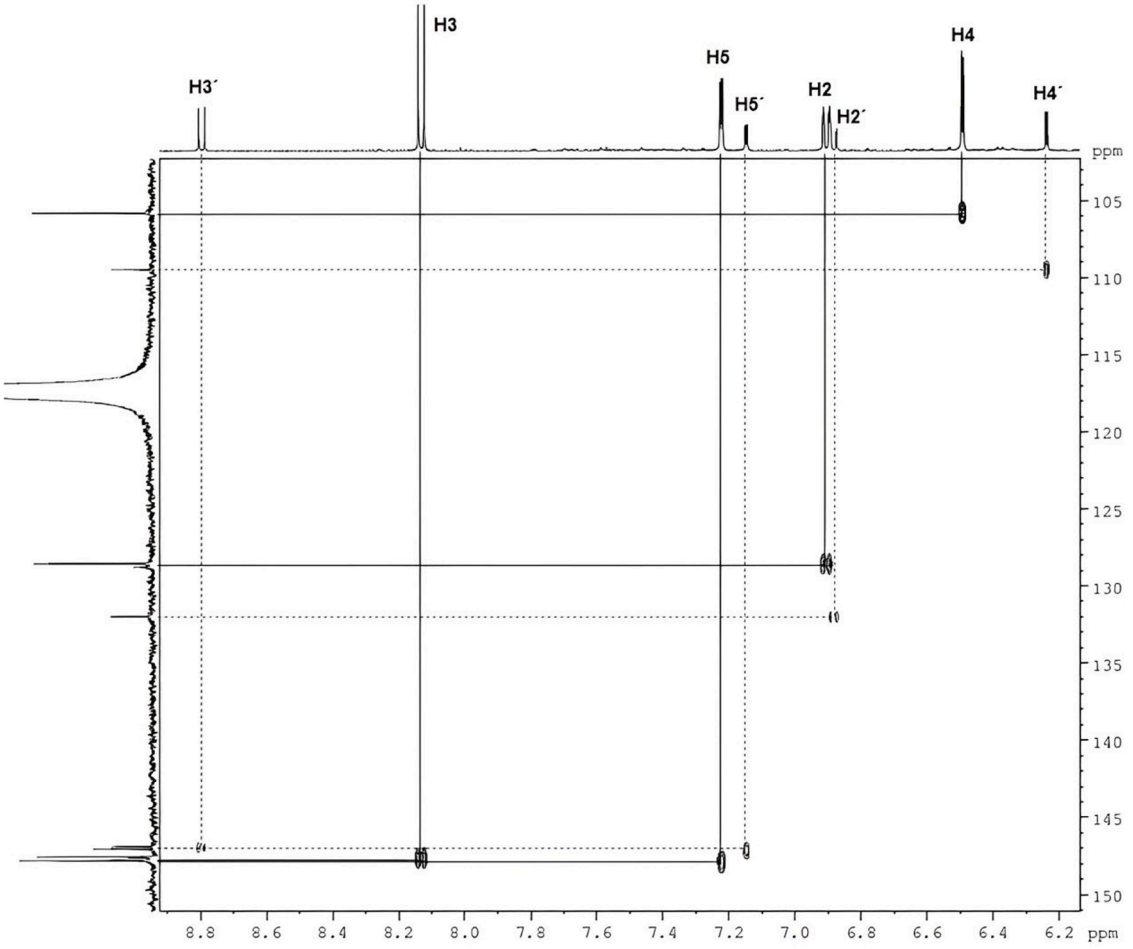

Fig. 9. HSQC contour map for PD1 dissolved in CD_3CN. Continuous lines indicate correlations corresponding to the substance in higher proportion, while dashed lines represent correlations for the substance in lower proportions.

Table 3
Chemical shifts (δ, ppm), coupling constants (J, Hz) and observed correlations for the major compound in photodegradation sample 1 (PD1) dissolved in CD_3CN, based on NMR and correlation spectroscopy analyses.

n	^1H	^{13}C / Type	^{13}C *	HMBC
1	–	168.1/ C	173.9	–
2	6.90 (ddd, *J*: 1.00, 1.95 and 10.60)	128.5/ -CH	132.9	105.8 and 168.1
3	8.13 (d, *J*: 10.60)	147.5/ -CH	143.1	128.5 and 147.5
4	6.49 (dd, *J*: 1.00 and 3.59)	105.8/ -CH	108.9	128.5, 147.5, 147.8 and 168.1
5	7.22 (dd, *J*: 1.95 and 3.59)	147.8/ -CH	144.0	105.8, 128.5, 147.8 and 168.1

* Chemical shifts estimated based on calculations performed using the software ACD/Lab.
d: doublet, dd: double doublet, ddd: doublet of doublets.

Table 4
Chemical shifts (δ, ppm), coupling constants (J, Hz) and correlations for the minor compound in photodegradation sample 1 (PD1) in CD_3CN.

n	^1H	^{13}C / Type	^{13}C*	HMBC
1′	–	166.3/ C	168.4	–
2′	6.88 (ddd, *J*: 0.55; 1.17 and 10.63)	132.0/ -CH	129.1	109.5, 146.9 147.1 and 166.3
3′	8.80 (d, *J*: 10.63)	146.9/ -CH	147.9	132.0
4′	6.24 (dd, *J*: 0.55 and 3.46)	109.5/ -CH	107.5	146.9, 147.1 and 166.3
5′	7.15 (dd, *J*: 1.17 and 3.46)	147.1/ -CH	147.8	109.5 and 166.3

* Chemical shifts estimated based on calculations performed using the software ACD/Lab.
d: doublet, dd: double doublet, ddd: doublet of doublets.

were observed for the PM G-0/SBE-β-CD, indicating its relative stability in the solid state during the assay period.

The photodegradation kinetics of the irradiated samples containing both cyclodextrin derivatives were monitored for at least three half-lives, with the results presented in Figs. 2 and 3.

Kinetic analysis of drug photodegradation, performed using the iteration method, indicating that the FDIC samples followed a first-order kinetic model. In contrast, the PM samples were better described by a zero-order kinetic model, suggesting distinct degradation pathway for the two types of samples. This observation is supported by the degradation curves shown in Figs. 2 and 3, as well the kinetic parameters summarized in Table 2.

A statistical comparison of the first-order FDIC complex kinetics for both SBE-β-CD and HP-β-CD derivatives, conducted using a T-test for independent curves, yielded a t-value of 0.4390 and a p-value of 0.3329, which are not statistically significant at $p < 0.05$. Similarly, the zero-order PM kinetics for both cyclodextrin derivatives under the same analytical conditions produced a t-value of 0.0603 and a p-value of 0.4763, also indicating no statistically difference between the kinetic curves at $p < 0$ 0.05. These findings highlight the consistency of the FDIC performance for both cyclodextrin derivatives, as evidenced by the

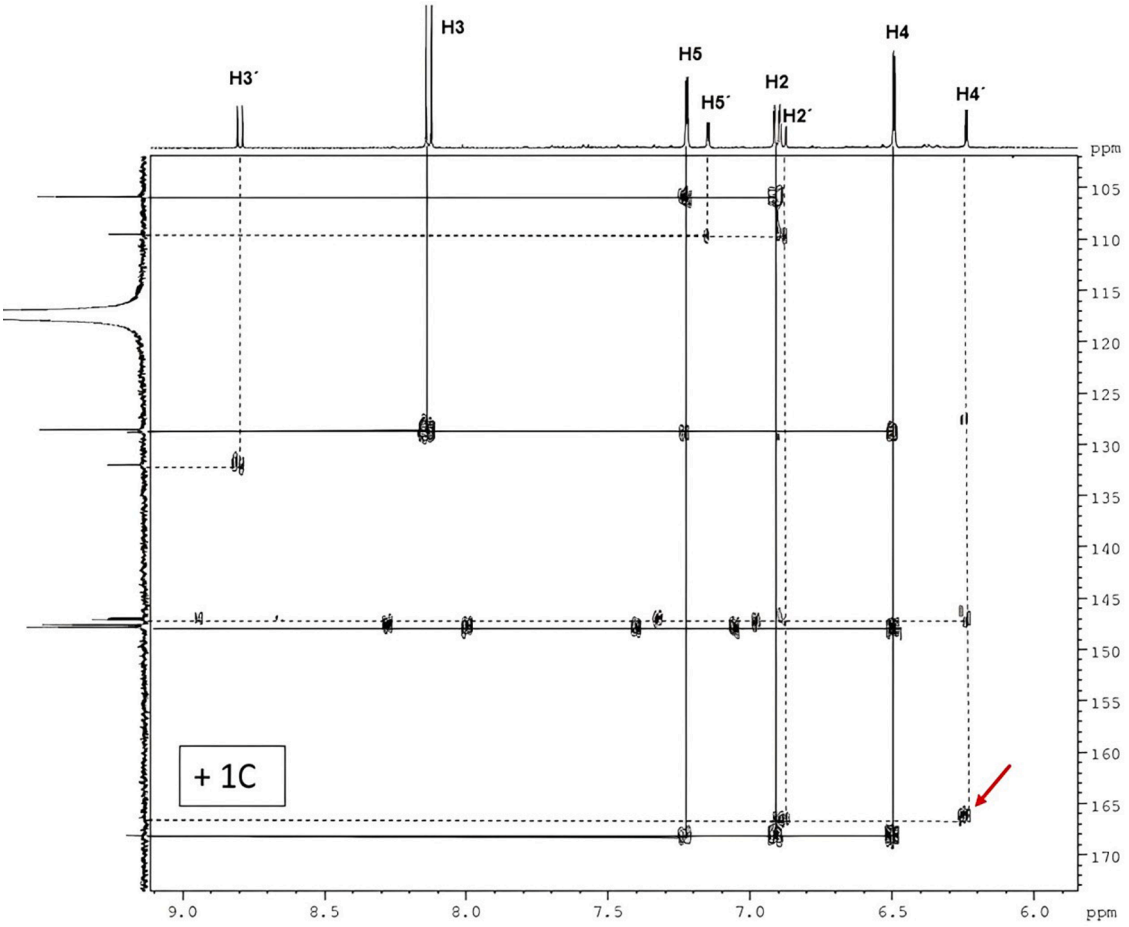

Fig. 10. HMBC contour map for PD1 dissolved in CD_3CN. Continuous and dashed lines indicate a correlation for the substances in higher and lower proportions, respectively. Notably, a signal from a carbon atom at 166.3 ppm, which was not observed in previous spectra, shows a correlation with H4' (indicated by an arrow).

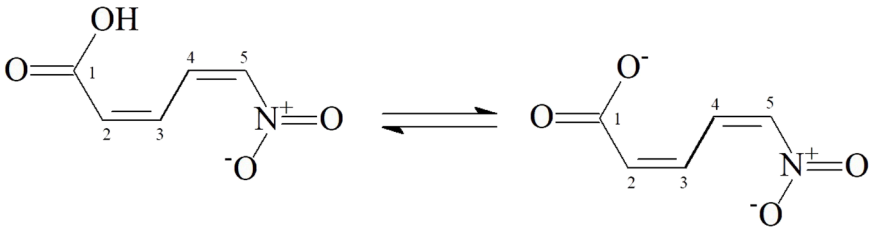

Fig. 11. Proposed chemical equilibrium between the structures of (2Z,4Z)-5-nitropenta-2,4-dienoic acid (NPDA, minor compound) and (2Z,4Z)-5-nitropenta-2,4-dienoate (major compound) present in photodegradation sample 1 (PD1). These structures result from the photodegradation of the freeze-dried inclusion complexes of G-0 with HP-β-CD and SBE-β-CD under light exposure.

similar first-order degradation rate constants and half-life times, suggesting a negligible impact on the photodegradation of complexed G-0 (Table 2).

3.2. Detection of G-0 and degradation products by HPLC

Under the experimental conditions, G-0 was eluted at 6.811 min with λ_{max} of 351 nm (Fig. 4A) and at lower intensity with a λ_{max} of 248 nm (Fig. 4B). According to a previous report, the primary photodegradation product obtained from crystalline G-0 was eluted at 7.5 min with a λ_{max} of 248 nm (de Rojas-Pérez, 2006). However, in the present study, this photoproduct was not detected in either of inclusion complexes (Fig. 4).

Interestingly, a prominent peak with a retention time of 5.4 min and a λ_{max} of 351 nm was identified in FDIC G-0/SBE-β-CD samples subjected to irradiation under photostability chamber conditions (ICH–Option 2). Additionally, minor peaks with retention times of 9.0 and 9.9 min were observed. In addition to the main photoproduct (PD1), minor peaks with retention times of 9.0 and 9.9 min were observed in the chromatographic profiles. Although their low abundance precluded isolation for NMR analysis, their presence suggests the formation of additional degradation products, possibly involving rearrangements or partial oxidation of the nitroalkene group. Further studies are warranted to elucidate their structures and toxicological relevance. These results indicate that the predominant photodegradation pathway of 2-(2-nitrovinyl)furan in solid inclusion complexes differs significantly from that in physical mixtures and crystalline drug forms (Fig. 5). The degradation profile observed under these conditions closely resembled the forced irradiation results, with minor variations attributable to the lower intensities of degradation product peaks (Supplementary data, Figure S1).

Table 5
In-silico toxicity assessment of 2-(2-nitrovinyl) furan (G-0) and its primary photodegradation product, (2Z,4Z)-5-nitropenta-2,4-dienoic acid (NPDA).

In Silico Test	Compounds	
Toxtree 3.1.0 estimation	**2-(2-nitrovinyl)furan**	**(2Z,4Z)-5-nitropenta-2,4-dienoic acid**
Cramer Rules	High (Class III)	High (Class III)
Verhaar Scheme	Class III (non-specific reactivity)	Class III (non-specific reactivity)
Carcinogenicity (genotoxic)	NO	NO
Carcinogenicity (non-genotoxic)	NO	NO
In vitro Mutagenicity (AMES)	NO	NO
Skin Sensitization Reactivity Domains	YES (Michael acceptor identified)	YES (Michael acceptor identified)
Structure (*in vivo* micronucleus assay in rodents)	NO	NO
Protein Binding Alerts	YES (Michael acceptor identified)	YES (Michael acceptor identified)
DNA Binding Alerts	YES (Michael acceptor identified)	NO
OSIRIS Property Explorer estimation	**2-(2-nitrovinyl)furan**	**(2Z,4Z)-5-nitropenta-2,4-dienoic acid**
Mutagenicity Risk	NO	NO
Tumorigenicity Risk	NO	NO
Irritating Effects Risk	NO	NO
Reproductive Effects Risk	NO	NO
pkCSM estimation		
Max Tolerate Dose (human) (log mg/kg/day)	0.867	0.502
Oral Rat Acute Toxicity (log mol/kg)	2.88	2.55
Oral Rat Chronic Toxicity (log mg/kg_bw/day)	1.683	1.106
Skin Sensitization	YES	YES
AMES Toxicity	NO	YES
hERG I Inhibitor	NO	NO
hERG II Inhibitor	NO	NO
preADMET estimation		
AMES Test	Mutagen	Mutagen
Carcinogenicity (Mouse)	Positive	Negative
Carcinogenicity (Rat)	Positive	Positive
In vitro hERG Inhibition	Medium risk	Low risk
T.E.S.T. 4.2.1 estimation		
Mutagenicity	NO	NO
Oral Rat LD50	ND	ND
ToxRead 0.23		
Mutagenicity	ND	Non mutagenic
Carcinogenicity	ND	ND
In vitro Micronucleus Assay	ND	ND
Skin Sensitization	ND	ND
QSAR Toolbox 4.4.1		
Toxic Hazard Classification	High (Class III)	High (Class III)
Oncologic Primary Classification	Nitroalkane and Nitroalkene Type Compounds	Nitroalkane and Nitroalkene Type Compounds
Carcinogenicity Alerts (genotoxic and non-genotoxic) alerts by ISS	No Alert Found	No Alert Found
DNA Alerts for AMES, *CA*, and MNT by OASIS	Radical	No Alert Found
In vitro Mutagenicity (AMES Test) Alerts by ISS	No Alert Found	No Alert Found
In vitro Mutagenicity (Micronucleus) Alerts by ISS	No Alert Found	No Alert Found
Protein Binding Alerts (Skin Sensitization – GHS)	Skin sensitization Category 1A	Skin sensitization Category 1A
Protein Binding Alerts (Chromosomal Aberration – OASIS)	No Alert Found	No Alert Found
Protein Binding Alerts (Skin Sensitization – OASIS)	Michael addition	Michael addition

ND = Not Determined.

3.3. Characterization of the main photoproduct (PD1) from solid inclusion complexes

The photodegradation products obtained from the solid inclusion complexes by light irradiation were separated using an LC/DAD system and further analyzed by NMR Spectroscopy. The ^{1}H NMR spectrum of the main photodegradation product (PD1) revealed eight signals in the chemical shift range of 6.24–8.8 ppm, displaying multiplicities (*d, dd, ddd*) consistent with highly conjugated systems (Fig. 6).

Additional signals were observed at 0.86 and 1.27 ppm, attributed to "grease" impurities, and at 1.91 ppm, which was assigned to the –CH_3 group from residual acetonitrile solvent (Supplementary Data, Figure S2).

Signal integration revealed the presence of two distinct spin systems, corresponding to two substances co-existing in the solution in a 1:3 ratio. Each system comprised four hydrogen signals, designated as H2 (H2), H3 (H3), H4 (H4), and H5 (H5), reflecting the observed similarities in their spectral patterns.

Analysis of ^{n}J-coupling constants indicated that coupling between H2-H3 and H2-H3' is consistent with a *cis* configuration. Additionally, the couplings observed between H2-H4, H2-H4; H2-H5, H2-H5' suggest either long-range (allylic) interactions or dihedral torsion angles approaching 90°

The presence of two hydrogen signals above 8 ppm, each corresponding to one of the substances, points to the influence of an electron-acceptor group attached to *An* sp^2 carbon. This group notably shifts the chemical environment of vinyl protons through π bonds resonance effects. Specifically, the vinyl hydrogen on the β-carbon of an α, β-unsaturated carbonyl system exhibits a higher deshielding (larger chemical shift value) compared to the α-carbon proton due to resonance effects.

Considering the original structure of the drug molecule (G-0), the nitro group serves as another potent electron-acceptor, likely retained in both substances. This group exerts a deshielding influence on the α-protons, further affecting their chemical shift values.

The ^{13}C {^{1}H} NMR, revealed nine signals between 109 and 168 ppm, corresponding to the analyzed compounds (Fig. 7). Impurities signals were detected at 0.5 and 29.3 ppm, and a cyan group from acetonitrile was identified at 117.3 ppm. Signals within the 100 to 150 ppm range were attributed to =*C*- type carbons, while the signal at 168 ppm is characteristic of carboxyl or carboxylate groups, consistent with the proton signals described earlier.

Notably, the hydrogen signals typical of carboxylic acids was absent in the ^{1}H NMR spectrum. This absence is likely due to a fast intermolecular proton exchange process, occurring at a rate beyond the detection capacity of the instrument.

Typically, weak signals in ^{13}C {^{1}H} NMR spectra may be obscured by noise, with hundreds of spectra removed and appearing only as an average. Consequently, the presence of certain carbon atoms may be needed to be inferred using other spectral techniques, such as Correlation Spectroscopy. From ^{1}H–^{1}H—COSY, direct connectivity was observed between H2-H3 (H2-H3) and H4-H5 (H4-H5) for both substances, as evidenced by cross peaks (Fig. 8).

Heteronuclear Single Quantum Coherence Spectroscopy (HSQC) further correlated carbon nuclei with directly attached protons ($^{1}J_{CH}$), with cross-peaks shown in Fig. 9. The correlation data, summarized in Tables 3 and 4, indicate that each carbon atom is bonded to a single proton (-CH). The absence of direct connectivity between carbons at 168.1 ppm or 166.3 ppm (depending on the substance) and protons corroborates the presence of a geminal carboxyl or carboxylate group. Additionally, the absence of –CH_2 groups in the molecules was verified, as these typically appear in an opposite phase to –CH and –CH_3 in the edited HSQC spectrum.

Heteronuclear Multiple Bond Coherence Spectroscopy (HMBC) was employed to detect correlations between hydrogen and carbon atoms over two and three bonds ($^{2}J_{CH}$ and $^{3}J_{CH}$), and occasionally over four bonds ($^{4}J_{CH}$), while preferentially suppressing direct correlations. Cross

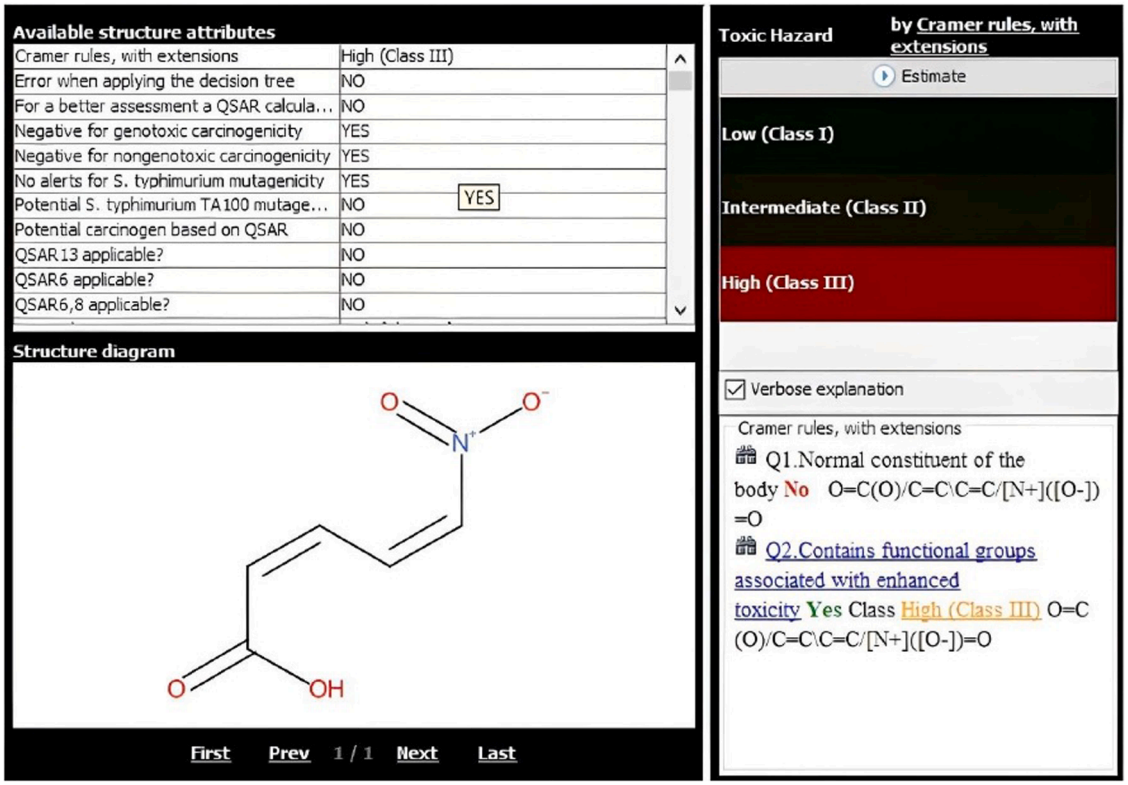

Fig. 12. Predicted toxicity profiles of (2Z,4Z)-5-nitropenta-2,4-dienoic acid (NDPA) generated using Toxtree 3.1.0 interface.

peaks observed in HMBC spectrum are shown in Fig.10, and the results are summarized in Tables 3 and 4.

Some expected signals were not detected in the HMBC spectrum. This absence may be attributed to various factors, including the bond dihedral angle, the type of orbitals involved, the selected long-distance coupling constant, or the number of scans used to acquire the spectrum (Silverstein et al., 2005).

Two direct correlations (C3-H3, C3′-H3′; C5-H5, C5′-H5′) were observed and appeared in the spectrum as two symmetric carbon signals associated with the specific hydrogen atoms. These correlations were also confirmed in the HSQC spectrum described previously.

Tables 3 and 4 present the assignments of chemical shifts (δ, ppm) and coupling constants (J, Hz) based on the data from ^{1}H and $^{13}C\{^{1}H\}$ NMR spectra, as well as correlations observed in the COSY, HSQC, and HMBC contour maps for both compounds. The proposed chemical equilibrium between (2Z,4Z)-5-nitropenta-2,4-dienoic acid (NPDA) and its conjugate base, (2Z,4Z)-5-nitropenta-2,4-dienoate, is illustrated in Fig. 11. These species coexist in the solution in a 1:3 ratio, corresponding to the minor and major compounds, respectively.

The photostabilization effects of drug G-0 through the formation of inclusion complexes have been extensively studied. However, such complexes do not always enhance the photostability of the guest molecule (Glass et al., 2001; Sortino et al., 2001; Tønnesen et al., 2002). 2-(2-nitrovinyl)furan is a photolabile compound in solid-state. Its primary degradation product was previously reported as a dimer, characterized by a maximum absorption wavelength at 248 nm in methanol/water (80:20, v/v) solution, and a molecular ion mass/charge ratio (m/z) of 277 using an LC-MS with an ESI interface in negative mode (de Rojas-Pérez, 2006). The formation of non-dimer photoproducts proposed in this study (Fig. 11) suggests that the dimerization reaction may be restricted due to the spatial geometry of the drug molecule within the hydrophobic cavity of these cyclodextrins. As previously demonstrated (Ruz et al., 2012), the inclusion complex limits intermolecular interactions of the drug without fully preventing its photodegradation. It is important to highlight that preliminary CG/MS analysis (data not shown) yielded an experimental ion at m/z 149.1, supporting the monomeric nature of the degradation product PD1, although full structural confirmation was obtained through detailed 1D and 2D NMR experiments.

Cyclodextrins possess a hydrophobic internal environment enriched with glycosidic oxygen atoms. The inclusion of guest molecules in their cavities can alter various physicochemical properties, including apparent solubility, spectral properties, and chemical reactivity. Cyclodextrins can influence the spatial orientation of molecules, as well as the rates of electron and proton transfer in the excited state and the overall decomposition rate of drugs (Chattopadhyay, 1991; Sur et al., 2000). During the evolution of photochemical intermediates, physical and chemical constraints can be imposed by the complexation process. The stoichiometry and geometry of the inclusion complexes significant influence the fundamental state of the molecules and the distribution of stable photoproducts (Moore, 2004).

Different cyclodextrin derivatives affect the photophysical characteristics of a drug molecule in diverse ways. For instance, some drugs may be stabilized when complexed with a particular cyclodextrin, while the same substance may become photolabile with another type of cyclodextrin. These differences are often attributed to variations in the conformations of the complexes, particularly in freeze-dried inclusion complexes (Ruz et al., 2012).

To the best of our knowledge, and based on a comprehensive search using the SciFinder database, this is the first report to propose the chemical structures of photoproducts generated under light exposure in the freeze-dried G-0 inclusion complexes with HP-β-CD and SBE-β-CD.

3.4. In silico evaluation of the toxicity of the main photoproduct (NDPA)

The biological activity and toxicity of nitro compounds, particularly nitro-aromatic and nitro-heteroaromatic drugs, have been extensively studied over the years. These investigations have established a relationship between the nitro group and the biological properties and toxicity of such compounds, with or without the involvement of

Table 6
Predicted Mutagenicity for (2Z,4Z)-5-nitropenta-2,4-dienoic acid (NPDA) using the Consensus method (T.E.S.T. 4.2.1).

Predictions for the chemical test and the six most structurally similar chemicals					
CAS	Structure	Similarity Coefficient	Experimental value	Predicted value	Endpoint
Chemical Test	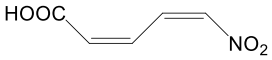 (NPDA)	–	–	0.38	Negative
699–18–3	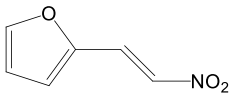 (G-0)	0.78	0.0	0.38	Negative
830–07–9	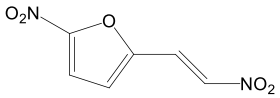	0.75	1.00	0.77	Positive
102–96–5	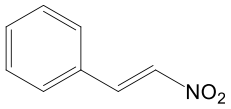	0.73	1.00	0.62	Positive
505–70–4	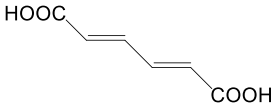	0.71	0.00	0.01	Negative
110–44–1	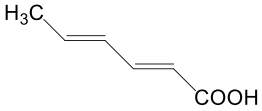	0.66	0.00	0.45	Negative
72,999–11–2	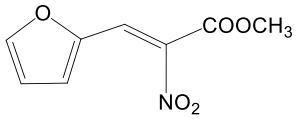	0.65	0.00	0.35	Negative

biotransformation processes affecting the nitro group (Kovacic and Somanathan, 2014; Paulai et al., 2009).

In general, the *in-silico* predictions indicated that both the parent compound (G-0) and the main photoproduct (NDPA) exhibit similar toxic potential (Table 5). Specifically, (2Z,4Z)-5-nitropenta-2,4-dienoic acid (NPDA) was classified as "Class 3″ by the Toxtree software (Fig. 12). Notably, the choice decision tree – whether the basic Cramer rules with extension or the revised Cramer decision tree - did not affect this classification. The assigned category results from Rule 2, which identifies the nitro group as a functional group associated with enhanced toxicity in chemical compounds.

The predictions for G-0 yielded similar results, likely due to the high structural similarity between the two compounds (Table 6), specifically the presence of the nitro-alkene fragment. Previous studies have critically reviewed the implementation of Cramer's Rules *in-silico* tools (Roberts et al., 2015). Among the tools employed, only preADMET classified both compounds as mutagens and carcinogens (in rats) while also estimating a moderate risk of hERG inhibition for G-0. The pkCSM method identified NPDA as positive for AMES toxicity, whereas G-0 was not, and suggested a reduced likelihood of hERG I/II inhibition for either compound. According to pkCSM, the photodegradation product (NPDA) exhibited higher toxicity, both qualitatively and quantitatively. In contrast, the other applications predict that both compounds are non-mutagenic and non-carcinogenic.

Toxtree 3.1.0 (Fig. 12) and QSAR Toolbox 4.4.1 (Fig. 13) flagged protein-binding alerts for both compounds and identified DNA alerts exclusively for G-0. Both methods also predict positive skin sensitization. Furthermore, QSAR Toolbox 4.4.1 classified both compounds as Category 1A sensitizers due to the presence of conjugated systems with electron-acceptor groups, such as the nitroalkene fragment.

Certain endpoints could not be determined by two of the methods employed, likely due to inconclusive results, low reliability of predictions, or cases falling outside the tools' application domains. Specifically, T.E.S.T. was unable to estimate the Oral Rat LD_{50}, while ToxRead 0.23 failed to assess the toxic potential of G-0 and only predicted the mutagenicity of NPDA (Fig. 14).

The toxicity of many chemical compounds (xenobiotics) often involves electrophilic reactions with endogenous nucleophiles (such as proteins and DNA) through the formation of covalent bonds, which alter the properties of these biomacromolecules.

The nucleophilic sites that can be attacked by electrophiles are ranked by their nucleophilic strength: 1) the thiol group of cysteine, 2) the sulfur atoms of methionine, 3) primary amino groups (*e.g.*, lysine, arginine), and 4) secondary amino groups, such as those of histidine in proteins. In DNA, the preferred nucleophilic sites include: 1) primary amino groups of purine bases (*e.g.* adenine, guanine), 2) ring nitrogen atoms of purine and pyrimidine bases (*e.g.* N7 of guanine), 3) oxygen atoms of purine and pyrimidine bases (*e.g.*, O6 of guanine), and 4) oxygen atoms of phosphate groups.

The initial chemical reactions that occur when an electrophilic xenobiotic covalently binds to a biomacromolecule can be grouped into various fundamental mechanistic domains: Michael addition, aromatic nucleophilic substitution (SNAr), unimolecular aliphatic nucleophilic substitution (SN_1), bimolecular aliphatic nucleophilic substitution (SN_2), Schiff base formation, acylation, and reactions involving free radicals (Aptula and Roberts, 2006; Schwöbel et al., 2011). However, not all electrophiles react with all potential biological nucleophiles. This selectivity is due to the numerous possible electrophilic reaction

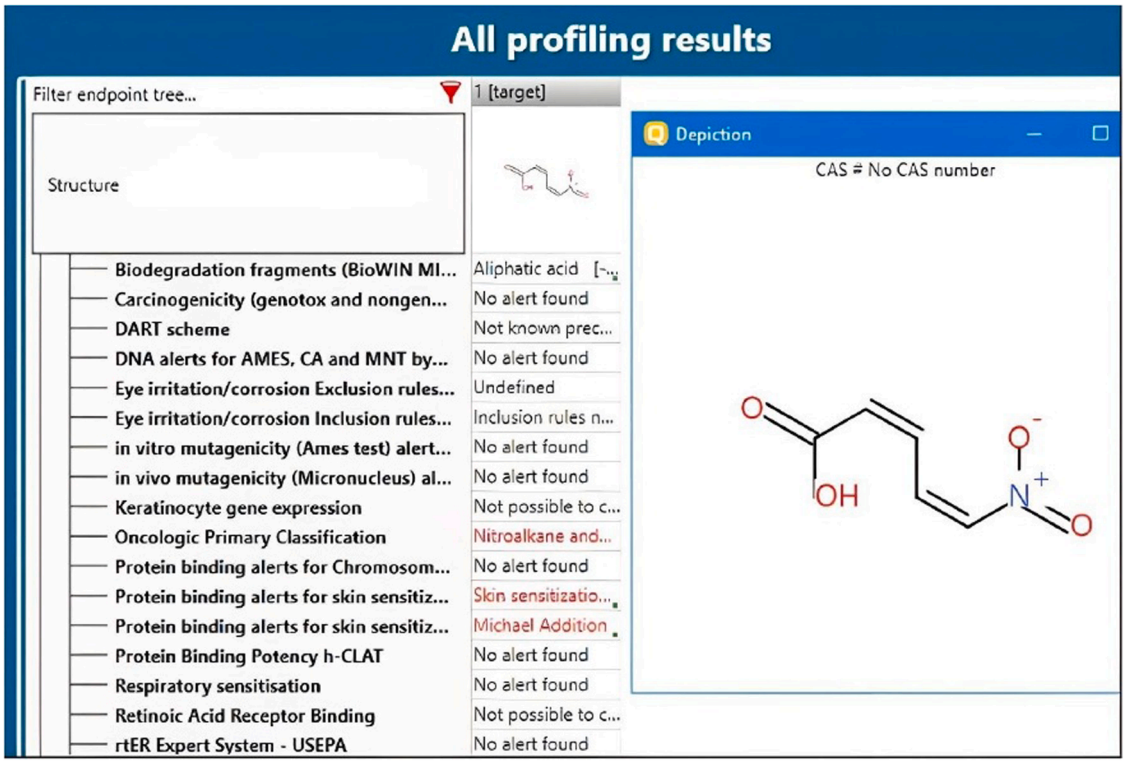

Fig. 13. Predicted toxicity profile of (2Z,4Z)-5-nitropenta-2,4-dienoic acid (NPDA) generated using QSAR Toolbox 4.4.1 interface.

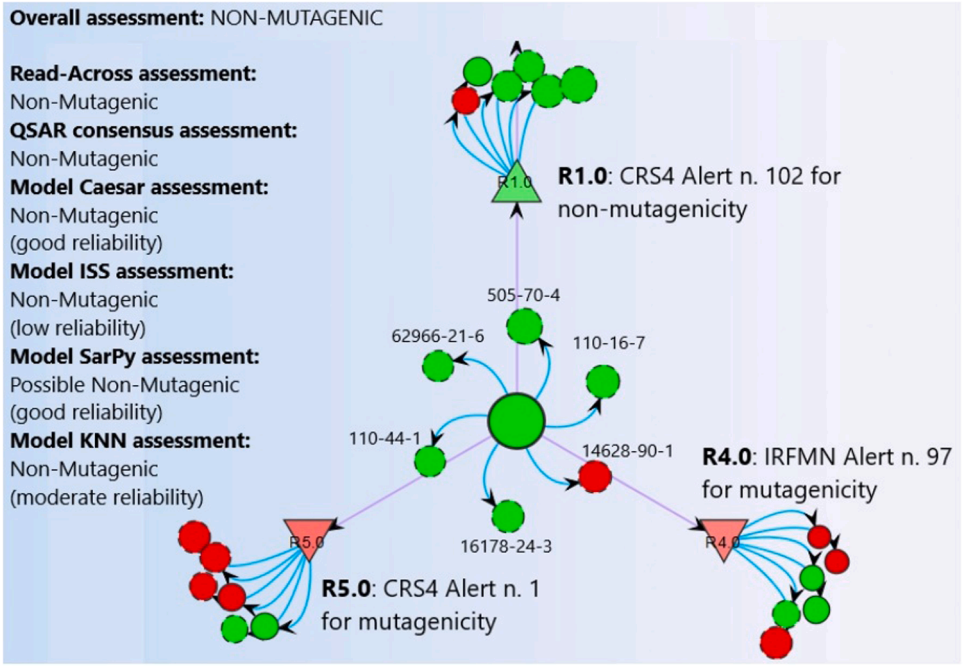

Fig. 14. Molecules decision tree, rules applied, and toxicity prediction for (2Z,4Z)-5-nitropenta-2,4-dienoic acid (NPDA) using the ToxRead 0.23 interface.

mechanisms and their varying rates of occurrence, resulting in different reactivity profiles toward specific nucleophilic sites in biological molecules.

Electrophiles and nucleophiles can be classified as "soft" or "hard" based on the polarizability. A “hard” electrophile typically has a localized electron deficiency, while a "soft" electrophile exhibits a delocalized electron deficiency across a larger molecular region. Hard electrophiles tend to react with DNA or amino groups, such as those in lysine, whereas soft electrophiles preferentially react with thiol groups, particularly cysteine in proteins. Electrophiles that act as Michael acceptors are considered weak electrophiles and preferentially attack proteins, making them more involved in skin irritation than mutagenic effects. In contrast, electrophiles capable of undergoing acylation reactions are considered strong electrophiles, with higher likelihood of reacting with strong DNA nucleophiles. This is a general reactivity pattern and does not apply to all cases (Schwöbel et al., 2011).

Table 7
Impurities Classification Based on Mutagenic and Carcinogenic Potential with Corresponding Control Actions (ICH M7) (ICH M7 2017).

Class	Definition	Proposed action for control
1	Known mutagenic carcinogens	Control at or below the compound-specific acceptable limit
2	Known mutagens with unknown carcinogenic potential (bacterial mutagenicity positive*, no rodent carcinogenicity data)	Control at or below acceptable limits (appropriate TTC)
3	Alerting structure, unrelated to the structure of the drug substance; no mutagenicity data	Control at or below acceptable limits (appropriate TTC) or conduct bacterial mutagenicity assay; If non-mutagenic = Class 5; If mutagenic = Class 2
4	Alerting structure, same alert present in the drug substance or related (*e.g.*, process intermediates) that have been tested and are non-mutagenic	Treat as the non-mutagenic impurity
5	No structural alerts, or an alerting structure with sufficient data demonstrating a lack of mutagenicity or carcinogenicity	Treat as the non-mutagenic impurity

Nitroalkenes are known to be reactive α, β-unsaturated organic compounds due to the strong electron-withdrawing effect of the nitro group on the hydrocarbon chain. This makes them electrophilic reagents that can attack proteins and nucleic acids, forming covalent bonds - a behavior known as Michael's acceptor reactivity (Aptula and Roberts, 2006). This reactivity can lead to protein or DNA damage, potentially causing sensitizing, irritating, or mutagenic effects (Schwöbel et al., 2011). However, the mere presence of nitro-α, β-unsaturated fragment in molecules such as NPDA and G-0, which constitutes a structural alert, does not necessarily indicate the manifestation of toxic effects. The presence and charge of substituent groups on the α and β carbon atoms can strongly influence the Michael reactivity (Schultz and Aptula, 2016; Wondrousch et al., 2010). Interestingly, the Michael reaction of nitroalkenes with thiol groups also mediates the cytoprotective and anti-inflammatory effects of nitroalkene fatty acids (Turell et al., 2018), showing that this reaction is not solely relevant from a toxicological perspective. The Michael reaction remains a subject of active research in the organic chemistry community (Hirahama et al., 2020; Li et al., 2020; Malkar et al., 2020; Wang et al., 2020; Zhang et al., 2020).

Analyzing the chemical structure of NPDA, it is a nitrodiene with a terminal carboxyl group, which also exerts electron-withdrawing effect, albeit weaker than the nitro group. The electronic conjugation along the carbon chain and the electron-withdrawing effect of the carboxyl group can delocalize the electrophilic center over a larger region, likely reducing the molecule's reactivity as a Michael acceptor. This suggests that the probability of NPDA reacting with DNA is low, and the primary toxicological concern would likely be as a potential skin sensitizer or irritant. Other chemical compounds structurally similar to NPDA exhibit varying toxic (mutagenic) effects depending on the substituents in their chemical structure (Table 6). This highlights that the mere presence of a nitroalkene group, although a structural alert, does not automatically correlate with the toxicity of a specific molecule.

Based on the structural factors influencing the reactivity of NPDA as Michael's acceptor and the consistent findings of the *in silico* toxicity prediction tools utilized in this study, NPDA can be classified as non-mutagenic and non-carcinogenic. However, caution is advised regarding potential skin irritation, particularly in topical pharmaceutical formulations. In such cases, it is recommended to take precautions against direct sunlight exposure. Finally, considering the structural alert identified and the similarity of NPDA to G-0, a known non-mutagenic compound, we propose assigning NPDA to Class 4 (Table 7).

4. Conclusions

2-(2-nitrovinyl)furan (G-0) undergoes degradation under the light conditions established by ICH, even when incorporated into freeze-dried inclusion complexes with HP-β-CD and SBE-β-CD. The main degradation product, identified through Nuclear Magnetic Resonance (NMR) analysis, was characterized as a mixture of (2Z,4Z)-5-nitropenta-2,4-dienoic acid (NPDA) and its corresponding salt form.

In silico toxicological screening using multiple computational methods predict that NPDA is non-mutagenic and non-carcinogenic. However, potential skin irritation effects are anticipated, necessitating appropriate precautions for the packaging, storage, and potential applications of the inclusion complexes.

CRediT authorship contribution statement

Vivian Ruz Sanjuan: Writing – original draft, Validation, Methodology, Investigation, Formal analysis, Data curation, Conceptualization. **Antonio Gilberto Ferreira:** Software, Methodology, Formal analysis. **Enoel Hernández Barreto:** Software, Methodology. **Guy Van den Mooter:** Writing – review & editing, Conceptualization. **Mirtha Mayra González Bedia:** Data curation. **Eryvaldo Socrates Tabosa do Egito:** Writing – review & editing, Visualization, Resources. **Anselmo Gomes de Oliveira:** Writing – review & editing, Writing – original draft, Supervision, Project administration, Funding acquisition, Formal analysis, Conceptualization.

Acknowledgments

The authors express their gratitude to AUIP-PAEDEX/UNESP-Brazil for providing the doctoral scholarship (V.R.S.). This research was supported by the National Research Council-CNPq-Brazil (A.G.O.), grant number 304617/2017-2, and the Coordination for Improvement of Higher Education Personnel (CAPES), grant number 001.

Special thanks to André Gonzaga dos Santos, Ph.D. (FCF-UNESP), for his assistance in preparing the cyclodextrins complexes, and to Alberto Cavalheiro, Ph.D., for technical support in isolating the photoproducts. We also acknowledge the Centro de Bioactivos Químicos-Cuba for providing the sample of the drug candidate (G-0) used in the study.

Supplementary materials

Supplementary material associated with this article can be found, in the online version, at doi:10.1016/j.ejps.2025.107238.

Data availability

No data was used for the research described in the article.

References

Ajiboye, T.O., 2018. 2-(2-Nitrovinyl) furan exacerbates oxidative stress response of *Escherichia coli* to bacteriostatic and bactericidal antibiotics. Microb. Pathog. 116, 130–134. https://doi.org/10.1016/J.MICPATH.2018.01.010.

Alabi, K…, Hassan, G., 2014. Determination of minimum inhibitory concentrations of 2-(2-nitrovinyl) furan. Acad. J. Microbiol. Res. 2, 28–32. https://doi.org/10.15413/ajmr.2014.0103.

Alabi, K.A., Owolabi, B., 2012. Synthesis and antimicrobial property of 2-(2-nitrovinyl) furan. J. Pure Appl. Microbiol. 6, 131–134.

Amberg, A., Beilke, L., Bercu, J., Bower, D., Brigo, A., Cross, K., Custer, L., Dobo, K., Dowdy, E., Ford, K., Glowienke, S., Van Gompel, J., Harvey, J., Hasselgren, C., Honma, M., Jolly, R., Kemper, R., Kenyon, M., Krublak, N., Leavitt, P., Miller, S., Muster, W., Nicolette, J., Plaper, A., Powley, M., Quigley, D., Vijavaraj-Reddy, M., Spirkl, H., Stavitskaya, L., Teasdale, A., Weiner, S., Welch, D., White, A., Wichard, J., Myatt, G., 2016. Principles and procedures for implementation of ICH M7 recommended (Q)SAR analysis. Regul. Toxicol. Pharmacol. 77, 13–24. https://doi.org/10.1016/j.yrtph.2016.02.004.

Aptula, A.O., Roberts, D.W., 2006. Mechanistic applicability domains for nonanimal-based prediction of toxicological end points: general principles and application to

reactive toxicity. Chem. Res. Toxicol. 19, 1097–1105. https://doi.org/10.1021/tx0601004.
Bhalekar, M.R., Harinarayana, D., Madgulkar, A.R., Pandya, S.J., Jain, D.K., 2008. Improvement of photostability in formulation: a review. Asian J. Chem. 20, 5095–5108.
Bienfait, B., Ertl, P., 2013. JSME: a free molecule editor in JavaScript. J. Cheminform. 5. https://doi.org/10.1186/1758-2946-5-24.
Bottini, A.A., Hartung, T., 2009. Food for thought on the economics of animal testing. ALTEX. 26, 3–16. https://doi.org/10.14573/altex.2009.1.3.
Chattopadhyay, N., 1991. Effect of cyclodextrin complexation on excited state proton transfer reactions. J. Photochem. Photobiol. a Chem. 58, 31–36. https://doi.org/10.1016/1010-6030(91)87096-E.
D'Auria, M., Emanuele, L., Mauriello, G., Racioppi, R., 2000. Photochemical dimerisation of 2-vinylfuran and 2-vinylthiophene derivatives bearing electron-withdrawing groups. J. Photochem. Photobiol. a Chem. 134, 47–154. https://doi.org/10.1016/S1010-6030(00)00260-4.
de Rojas-Pérez, M., 2006. Estudio de los Productos de Degradación del 2-(2-nitrovinil) Furano (Gg-0). Universidad de Cádiz. Available at https://dialnet.unirioja.es/servlet/tesis?codigo=52039.
Fjodorova, N., Novic, M., 2012. Integration of QSAR and SAR methods for the mechanistic interpretation of predictive models for carcinogenicity. Comput. Struct. Biotechnol. J. 1. https://doi.org/10.5936/csbj.201207003.
Glass, B.D., Brown, M.E., Daya, S., Worthington, M.S., Drummond, P., Antunes, E., Lebete, M., Anoopkumar-Dukie, S., Maharaj, D., 2001. Influence of cyclodextrins on the photostability of selected drug molecules in solution and the solid-state. Int. J. Photoenergy 3, 205–211. https://doi.org/10.1155/S1110662×01000277.
González Borroto, J.I., Creus, A., Marcos, R., 2001. Genotoxic evaluation of the furylethylene derivative 2-furyl-1-nitroethene in cultured human lymphocytes. Mutat. Res. 497, 177–184. https://doi.org/10.1016/S1383-5718(01)00262-5.
González Borroto, J.I., Machado, G.Pérez, Creus, A., Marcos, R., 2005. Comparative genotoxic evaluation of 2-furylethylenes and 5-nitrofurans by using the comet assay in TK6 cells. Mutagenesis. 20, 193–197. https://doi.org/10.1093/mutage/gei026.
Gonzalez Borroto, J.I., Creus, A., Marcos, R., Molla, R., Zapatero, J., 2003. The mutagenic potential of the furylethylene derivative 2-furyl-1-nitroethene in the mouse bone marrow micronucleus test. Toxicol. Sci. 72, 359–362. https://doi.org/10.1093/toxsci/kfg038.
Hirahama, T., Umezawa, M., Shoji, M., 2020. Photoredox Michael addition of phenylmalononitrile onto α,β-unsaturated carboxylic acid. Tetrahedron. Lett. 61. https://doi.org/10.1016/j.tetlet.2020.151824.
ICH, International conference on harmonization of technical requirements for registration of pharmaceuticals for human use (ICH). (Q1B) stability testing: photostability testing of new drug substances and products, (1996). https://database.ich.org/sites/default/files/Q1BGuideline.pdf (accessed January 6, 2021).
ICH M7, ICH guideline M7(R1) on assessment and control of DNA reactive (mutagenic) impurities in pharmaceuticals to limit potential carcinogenic risk, (2017). https://www.ema.europa.eu/en/documents/scientific-guideline/ich-guideline-m7r1-assessment-control-dna-reactive-mutagenic-impurities-pharmaceuticals-limit_en.pdf (accessed January 6, 2021).
ICH Q3A, ICH, Q3A (R2): Impurities in new drug substances, International Conference on Harmonization, Geneva., Available from ⟨http//Www.Ich.Org/Fileadmin/Public_Web_Site/ICH_Products/Guidelines/Quality/Q3A_R2/Step4/Q3A_R2__Guideline.Pdf⟩. (2006). https://database.ich.org/sites/default/files/Q3A(R2)Guideline.pdf.
Kolarević, A., Kocić, G., Yancheva, D., Šmelcerović, A., 2016. *In silico* pharmacokinetic and toxicological study of DNAse inhibitors. Acta Med. Median 55, 5–13. https://doi.org/10.5633/amm.2016.0401.
Kovacic, P., Somanathan, R., 2014. Nitroaromatic compounds: environmental toxicity, carcinogenicity, mutagenicity, therapy and mechanism. J. Appl. Toxicol. 34, 810–824. https://doi.org/10.1002/jat.2980.
Li, Q.-F., Chu, S., Li, E., Li, M., Wang, J.-T., Wang, Z., 2020. Lanthanide-based hydrogels with adjustable luminescent properties synthesized by thiol-Michael addition. Dye. Pigment. 174. https://doi.org/10.1016/j.dyepig.2019.108091.
Luechtefeld, T., Marsh, D., Rowlands, C., Hartung, T., 2018. Machine learning of toxicological big data enables read-across structure activity relationships (RASAR) outperforming animal test reproducibility. Toxicol. Sci. 165, 198–212. https://doi.org/10.1093/toxsci/kfy152.
Malkar, R.S., Jadhav, A.L., Yadav, G.D., 2020. Innovative catalysis in Michael addition reactions for C-X bond formation. Mol. Catal. 485. https://doi.org/10.1016/j.mcat.2020.110814.
Manganelli, S., Benfenati, E., Manganaro, A., Kulkarni, S., Barton-Maclaren, M., Honma, T.S., 2016. New quantitative structure–Activity relationship models improve predictability of Ames mutagenicity for aromatic azo compounds. Toxicol. Sci. 153, 316–326. https://doi.org/10.1093/toxsci/kfw125.
Moore, D.E., 2004. Standardization of kinetic studies of photodegradation reactions. In: Tønnesen, H.H. (Ed.), Photostability Drugs Drugs Formul, 2nd ed. Washington, pp. 42–64.
Myatt, G…, Ahlberg, E., Akahori, Y., Allen, D., Amberg, A., Angere, L…, Aptula, A., Auerbach, S., Beilkeh, L., Bellioni, P., Benigni, R., Bercu, J., Booth, E…, Bower, D., Brigo, A., Burden, N., Cammerer, Z., Cronin, M.T.D., Cross, K.P., Custer, L., Dettwiler, M., Dobo, K., Ford, K.A., Fortin, M.C., Gad-McDonald, S…, Gellatly, N., Gervais, V., Glover, K.P., Glowienke, S., Van-Gompelz, J., Gutsell, S., Hardy, B., Harvey, J.S., Hillegass, J., Honmacc, M., Hsiehdd, J.-H., Hsuee, C.-W., Hughesff, K., Johnsona, C., Jollygg, R., Joneshh, D., Kemperii, R., Kenyons, M.O., Kimee, M.T., Kruhlakee, N.L., Kulkarniff, S.A., Kümmererjj, Klaus, Leavittq, P., Majerkk, B., Masteng, S., Millera, S., Moserll, J., Mm, M.M., Muster, W., Neilsono, L., Opreap, T. I., Patlewiczqq, G., Paulinorr, A., Lo Pipaross, E., Powleyee, M., Quigleya, D.P., Reddytt, M.V., Richarzuu, A.-N., Ruiznn, P., Schilterss, B., Serafimovavv, R., Simpsonf, W., Lidiya Stavitskayaee, R.S., Suarez-Rodriguez, D., Szabo, D.T., Teasdale, A., Trejo-Martin, A., Valentiny, J.-P., Vuorineni, A., Wallz, B.A., Wattsaaa, P., Whitebb, A.T., Wichardbbb, J., Wittg, K.L., Woolleyccc, A., Woolleyccc, D., Zwicklddd, C., Hasselgrena, C., 2018. *In silico* toxicology protocols. J. Regul. Toxicol. Pharmacol. 16, 1–17. https://doi.org/10.1016/j.yrtph.2018.04.014.
E. Olazábal-Manso, N. Castañedo-Cancio, T. Gaitán-Placeres, Z. Rodríguez-Negrín, O. Hernández, H. Serrano-Pérez, M.I. Diaz-Molina, A.M. Calvo-Alonso, Method of obtaining 2-(2-nitrovinyl)-furan and the use thereof as a coccidiostatic, (2002).
Paulai, F.R., Serrano, S.H.P., Tavares, L.C., 2009. Aspectos mecanísticos da bioatividade e toxicidade de nitrocompostos. Quim. Nova 32, 1013–1020. https://doi.org/10.1590/S0100-40422009000400032.
Popielec, A., Loftsson, T., 2017. Effects of cyclodextrins on the chemical stability of drugs. Int. J. Pharm. 531, 532–542. https://doi.org/10.1016/j.ijpharm.2017.06.009.
Raies, A.B., Bajic, V.B., 2016. *In silico* toxicology: computational methods for the prediction of chemical toxicity. WIREs Comput. Mol. Sci. 6, 147–172. https://doi.org/10.1002/wcms.1240.
Roberts, D.W., Aptula, A., Schultz, T.W., Shen, J., Api, A.M., Bhatia, S., Kromidas, L., 2015. A practical guidance for Cramer class determination. Regul. Toxicol. Pharmacol. 73, 971–984. https://doi.org/10.1016/j.yrtph.2015.09.017.
Ruz, V., Froeyen, M., Busson, R., González, M.M., Baudemprez, L., Van den Mooter, G., 2012. Characterization and molecular modeling of the inclusion complexes of 2-(2-nitrovinyl) furan (G-0) with cyclodextrines. Int. J. Pharm. 439, 275–285. https://doi.org/10.1016/j.ijpharm.2012.09.025.
Ruz, V., González, M., Winant, D., Rodríguez, Z., Van den Mooter, G., Ruz, V., González, M.M., Winant, D., Rodríguez, Z., den Mooter, G.Van, 2015. Characterization of the sublimation and vapor pressure of 2-(2-Nitrovinyl) furan (G-0) using thermogravimetric analysis: effects of complexation with cyclodextrins. Molecules. 20, 15175–15191. https://doi.org/10.3390/molecules200815175.
Ruz-Sanjuan, V., Van den Mooter, G., Zeppone-Carlos, I., dos Santos-Ramos, M., Bauab, T., Bergamaschi-Tercini, A., González-Bedia, M., Oliveira, A.G., 2020. Stability, biological and biopharmaceutical evaluation of the inclusion complexes of the antifungal and antiprotozoal drug candidate 2-(2-nitrovinyl) furan (G-0) with beta-cyclodextrin derivatives. J. Drug Deliv. Sci. Technol. 58, 101767. https://doi.org/10.1016/j.jddst.2020.101767.
Schmidt, F., 2021. Computational toxicology. Syst. Med. 2, 283–300. https://doi.org/10.1016/B978-0-12-801238-3.11534-X.
Schultz, T.W., Aptula, A.O., 2016. Kinetic-based reactivity for Michael Acceptors: structural activity relationships and its relationship to excess acute fish toxicity. Bull. Environ. Contam. Toxicol. 97, 752–756. https://doi.org/10.1007/s00128-016-1871-y.
Schwöbel, J.A.H., Koleva, Y.K., Enoch, S.J., Bajot, F., Hewitt, M., Madden, J.C., Roberts, D.W., Schultz, T.W., Cronin, M.T.D., 2011. Measurement and estimation of electrophilic reactivity for predictive toxicology. Chem. Rev. 111, 2562–2596. https://doi.org/10.1021/cr100098n.
Sifontes-Rodríguez, S., Monzote-Fidalgo, L., Castañedo-Cancio, N., Montalvo-Álvarez, A. M., López-Hernández, Y., Diogo, N.M., Infante-Bourzac, J.F., Pérez-Martín, O., Meneses-Marcel, A., García-Trevijano, J.A.E., Cabrera-Pérez, M.Á., 2015. The efficacy of 2-nitrovinylfuran derivatives against Leishmania *in vitro* and *in vivo*. Mem. Inst. Oswaldo Cruz. 110, 166–173. https://doi.org/10.1590/0074-02760140324.
S. Sifontes-Rodríguez, Descubrimiento racional de compuestos químicos para el tratamiento de la leishmaniosis y la enfermedad de Chagas, E-Prints Complutense, 2017.
Silverstein, R.M., Webster, F.X., Kiemle, D.J., 2005. Spectrometric Identification of Organic Compounds.
Sortino, S., Giuffrida, S., De Guldi, G., Chillemi, R., Petralia, S., Marconi, G., Condorelli, G., Sciuto, S., 2001. The photochemistry of flutamide and its inclusion complex with beta-cyclodextrin. Dramatic effect of the microenvironment on the nature and on the efficiency of the photodegradation pathways. Photochem. Photobiol. 73, 6–13. https://doi.org/10.1562/0031-8655(2001)073<0006:tpofai>2.0.co;2.
Stanton, K., Kruszewski, F.H., 2016. Quantifying the benefits of using read-across and *in silico* techniques to fulfill hazard data requirements for chemical categories. Regul. Toxicol. Pharmacol. 81, 250–259. https://doi.org/10.1016/j.yrtph.2016.09.004.
Sur, D., Purkayastha, P., Chattopadhyay, N., 2000. Kinetics of the photoconversion of diphenylamine in β-cyclodextrin environments. J. Photochem. Photobiol. a Chem. 134, 17–21. https://doi.org/10.1016/S1010-6030(00)00241-0.
Tønnesen, H.H., Másson, M., Loftsson, T., 2002. Studies of curcumin and curcuminoids. XXVII. Cyclodextrin complexation: solubility, chemical and photochemical stability. Int. J. Pharm. 244, 127–135. https://doi.org/10.1016/s0378-5173(02)00323-x.
Tourneix, F., Alépée, N., Detroyer, A., Eilstein, J., Ez-Zoubir, M., Teissier, S.M., Noçairi, H., Piroird, C., Basketter, D., Bufalo, A.D., 2010. Skin sensitisation testing in practice: applying a stacking meta model to cosmetic ingredients. Toxicol. Vitr. 66. https://doi.org/10.1016/j.tiv.2020.104831.
Turell, L., Steglich, M., Alvarez, B., 2018. The chemical foundations of nitroalkene fatty acid signaling through addition reactions with thiols. Nitric. Oxide 78, 161–169. https://doi.org/10.1016/j.niox.2018.03.014.
Verheyen, G.R., Braeken, E., Deun, K.V., Miert, S.V., 2017. Evaluation of existing (Q)SAR models for skin and eye irritation and corrosion to use for REACH registration. Toxicol. Lett. 265, 47–52. https://doi.org/10.1016/j.toxlet.2016.11.007.
Wang, S., Yan, L.C., Zheng, S.S., Li, T.T., Fan, L.Y., Huang, T., Li, C., Zhao, Y.H., 2019. Toxicity of some prevalent organic chemicals to tadpoles and comparison with toxicity to fish based on mode of toxic action. Ecotoxicol. Environ. Saf. 167. https://doi.org/10.1016/j.ecoenv.2018.09.105.

Wang, T., Han, Y., Bai, Y., Zhu, Q., Quan, D., Liu, X., 2020. Poly(ether-carbonate) based hydrogel with tunable mechanical strength and enhanced bioactivity prepared by Michael addition. Polymer. (Guildf) 188. https://doi.org/10.1016/j.polymer.2019.122115.

Wondrousch, D., Böhme, A., Thaens, D., Ost, N., Schüürmann, G., 2010. Local electrophilicity predicts the toxicity-relevant reactivity of Michael Acceptors. J. Phys. Chem. Lett. 1, 1605–1610. https://doi.org/10.1021/jz100247x.

Yeni, S., Merdekawati, F., 2018. *In silico* toxicity prediction of 1-phenyl-1-(quinazolin-4-yl) ethanol compounds by using Toxtree, pkCSM and preADMET. Pharmaciana 8, 2015–2016. https://doi.org/10.12928/pharmaciana.v8i2.9508.

Yuan, L., Li, S., Huo, D., Zhou, W., Wang, X., Bai, D., Hu, J., 2018. Studies on the preparation and photostability of Avobenzone and (2-hydroxy)propyl-beta-cyclodextrin inclusion complex. J. Photochem. Photobiol. a Chem. https://doi.org/10.1016/j.jphotochem.2018.09.036.

Zhang, Z., Dai, S., Li, L., Jia, C., Zhang, Y., Li, H., 2020. Scandium-catalyzed Michael addition of quinazolinones and vinylazaarenes. Tetrahedron. Lett. 61. https://doi.org/10.1016/j.tetlet.2020.151926.

Zhuang, J., Xing, X., Wang, D., Du, Z., Wang, J., Dong, Y., Yu, W., Siyal, S.H., 2018. Toxicity assessment of the extractables from multi-layer coextrusion polyethylene bags exposed to pH=5 solution containing 4% benzyl alcohol and 0.1 M sodium acetate. Regul. Toxicol. Pharmacol. 94, 47–56. https://doi.org/10.1016/j.yrtph.2018.01.015.